Design and Analysis of Stand-alone DC Powered Photovoltaic System: (The Case of Multi-Service Access Gateway in Adama)

By: Tewodros Tilahun Gebere

A Thesis Submitted to

The Department of Electrical Power and Control Engineering

School of Electrical Engineering and Computing

Presented in Partial Fulfillment of the Requirement for the Master of Science Degree in Electrical Power Engineering

Office of Graduate Studies

Adama Science and Technology University

June, 2022

Adama, Ethiopia

Design and Analysis of Stand-alone DC Powered Photovoltaic System: (The Case of Multi-Service Access Gateway in Adama)

By: Tewodros Tilahun Gebere

Advisor: Dr. Tefera Terefe Yitayew

A Thesis Submitted to
The Department of Electrical Power and Control Engineering
School of Electrical Engineering and Computing

Presented in Partial Fulfillment of the Requirement for the Master of Science Degree in Electrical Power Engineering

Office of Graduate Studies

Adama Science and Technology University

June, 2022

Adama, Ethiopia

DECLARATION

I hereby declare that this Master Thesis entitled “Design and Analysis of Stand-alone DC Powered Photovoltaic System: (The Case of Multi-Service Access Gateway in Adama)” is my original work. That is, it has not been submitted for the award of any academic degree, diploma, or certificate in any other university. All sources of materials that are used for this thesis have been duly acknowledged through citation.

________________________	________________________	_______________
Name of Student	Signature	Date

RECOMMENDATION

We, the advisors of this thesis, hereby certify that we have read the revised version of the thesis entitled "Design and Analysis of Stand-alone DC Powered Photovoltaic System: (The Case of Multi-Service Access Gateway in Adama)" prepared under our guidance by Tewodros Tilahun Gebere submitted in partial fulfillment of the requirements for the degree of Masters of Science in electrical power and control engineering (Power). Therefore, we recommend the submission of the revised version of the thesis to the department following the applicable procedures.

______________________________	____________	___________
Advisor	Signature	Date

APPROVAL SHEET

We, the advisors of this thesis entitled "Design and Analysis of Stand-alone DC Powered Photovoltaic System: (The Case of Multi-Service Access Gateway in Adama)" and developed by **Tewodros Tilahun Gebere,** hereby certify that the recommendations and suggestions made by the board of examiners are appropriately incorporated into the final version of the thesis.

______________________	______________________	______________________
Advisor	Signature	Date

We, the undersigned, members of the Board of Examiners of the thesis by **Tewodros Tilahun Gebere** have read and evaluated the thesis entitled "Design and Analysis of Stand-alone DC Powered Photovoltaic System: (The Case of Multi-Service Access Gateway in Adama)" and examined the candidate during open defense. This is, therefore, to certify that the thesis is accepted for partial fulfillment of the requirement of the degree of Master of Science in Electrical Power and Control Engineering (Power).

______________________	______________________	______________________
Chairperson	Signature	Date
______________________	______________________	______________________
Internal Examiner	Signature	Date
______________________	______________________	______________________
External Examiner	Signature	Date

Finally, approval and acceptance of the thesis is contingent upon submission of its final copy to the Office of Postgraduate Studies (OPGS) through the Department Graduate Council (DGC) and School Graduate Committee (SGC).

______________________	______________________	______________________
Department Head	Signature	Date
______________________	______________________	______________________
School Dean	Signature	Date
______________________	______________________	______________________
Office of Postgraduate Studies, Dean	Signature	Date

ACKNOWLEDGEMENT

First and foremost, I would like to express my most heartfelt and profound gratitude to my supervisor, **Dr. Tefera Terefe Yitayew** for his unlimited professional guidance and support throughout my research. I thank him not only for his valuable advice on my research work but also, for his help in personal matters. He was much more than an academic supervisor to me.

I am also very grateful to **Mr. Minyamer Gelawe Wase** (**MSc.**) for his encouragements, advice, unwillingness support, and helping in editing the thesis documentation and implementing the system in Simulink in general.

I would moreover like to thank my colleague and friend **Mr. Demsachew Lemma** for his patience, helpful attitude, and unwillingness support, patience, and encouragement throughout my research work.

Furthermore, I am also very grateful to all Electrical Power and Control Engineering department staff members for their unwillingness support, patience, and encouragement throughout my research work.

Finally, I am also very grateful to my whole family and friends who supported me directly or indirectly. Most of all I would like to thank the almighty God who I strongly believe gave me the power and the strength to accomplish this task.

TABLE OF CONTENTS

LIST OF TABLES

LIST OF FIGURES

LIST OF ACRONYMS

Abbreviations	**Descriptions**
AC	Alternating Current
APOD	Alternative Phase Opposition Disposition
CCM	Continues Conduction Mode
DC	Direct Current
DCM	Discontinuous Conduction Mode
GTO	Gate Turn Off Thyristor
IGBT	Insulated Gate Bipolar Transistor
MSAG	Multi-Service Access Getway
MOSFET	Metallic Oxide Silicon Field Effect Transistor
MPPT	Maximum Power Point Tracker
OCPD	Over Current Protective Device
P&O	Perturb and Observe
PID	Proportional Integral Derivative
PWM	Pulse Width Modulation
SCR	Silicon Controlled Rectifier

LIST OF SYMBOLS

Symbol	Description
E_g	Band Gap Energy
G	Solar Insolation
G_o	Extra-terrestrial Radiation on Horizontal Surface
G_{on}	Extra-terrestrial Radiation, Measured on the Plane Normal to the Radiation
G_{ref}	Reference Solar Insolation
H	Monthly Average Daily Radiation
H_o	Daily Extra-terrestrial Radiation on Horizontal Surface
I	Output Current
I_d	Diode Saturation Current
I_{ph}	Photon Generated Current
I_{RS}	Reverse Saturation Current
I_s	Saturation Current
I_{sc}	Short Circuit Current
I_{sh}	Shunt Current
K	Boltzmann Constant
K_i	Short Circuit Current Temperature Coefficient
N	Diode Ideality Factor
n	Sunshine Hours
N	Maximum Possible Daily Hours of Bright Sunshine
n_d	n^{th} Day of the Year
N_p	Number of Cells Connected in Parallel
N_s	Number of Cells Connected in Series
Q	Electron Charge
R_s	Series Resistance
R_{sh}	Shunt Resistance
T_c	Cell Temperature
T_{ref}	Reference Temperature
V	Output Voltage

V_{oc}	Open Circuit Voltage
V_T	Thermal Voltage
α_s	Solar Altitude Angle
Β	Slope
Γ	Surface Azimuth Angle
γ_s	Solar Azimuth Angle
Δ	Declination Angle
Θ	Angle of Incidence
θ_z	Zenith Angle
Φ	Latitude
Ω	Hour Angle
ω_s	Sun Rise/Sun Set Angle

ABSTRACT

The ability to use renewable energy resources has been grown continuously over the past few decades due to global warming and the depletion of fossil fuels. These fundamental things have initiated researchers to do scientific research into it. Multi-Service Access Gateway (MSAG) are one of the access layers of telecom services in the country specifically for the wired cellphones and internet applications as an example. The device usually supplied from the main grid system. Due to power fluctuation and interruption, it may not give services to the customer. Solar energy is an alternative solution to replace the dependency of the main grid supply. However, it needs an appropriate control of the system voltage and requires energy storages. In this research thesis, the design and analysis of stand-alone solar powered Multi-Service Access Gateway for Ethio-telecom was carried out using MATLAB and HOMER softwares. In this regard, the components of standalone photovoltaic based MSAG system such as, Photovoltaic panel, DC-DC boost converter with regulator, DC-DC bidirectional converter, battery modeling, and cable sizes are carefully sized to design the system. In addition, the total cost per kWh is also determined both in mathematical and HOMER software and its result is $0.258/kWh. To achieve this the mathematical modeling of the PV, DC-DC converters, and battery system has been done. In order to truck the maximum power, an MPPT based on P&O algorithm is applied. For regulating the voltage in the DC-DC converter a PID controller is used. Also, for the implementation purpose the energy demand of deferable load 80.34kWh/day with peak load of 4.06kW has been involved during HOMER optimization. Furthermore, a detailed electrical characteristic of 48V PV array with 3 series and 51 parallel configurations was determined on I-V and P-V plane by taking manufacturer's data sheet of the PV module as input.

***Keywords**: MSAG, PV, DC-DC converters, and Energy storage batteries.*

CHAPTER ONE

INTRODUCTION

1.1. Background

The telecommunication industry is one of the fastest developing businesses within the world. The unforeseen increment in endorsers and demand for telecommunication services has driven huge development in telecommunication systems. In Ethiopia, Ethio-telecom was established in November 2010 by supplanting the past title of the company Ethiopian Telecommunications Corporation (ETC). The company has passed through diverse names since 1894 E.C at the governance of Emperor Menelik II when the 407 Km telegraph line between the cities of Harar and the capital Addis Ababa was developed (Baron et al., 2010).

As of now, Ethio-telecom is the sole service supplier of telecom technology within the whole nation with comprehensive plans in put to meet the prerequisites set out by the Council of Ministers. The Federal Government of Ethiopia claimed and controlled all broadcast communications services, except selling of Customer Premises Equipment (CPE) (ethiotelecom, 2020).

To supply solid and secured communication services at a reasonable price all through the nation, the company has developed broad mixed-capability Information Communication Technology (ICT) infrastructure that gives a mixed scope of 85% of the country’s population, with the potential to serve 90% of its population. Over 500 cities have been associated with fixed-line Internet and each territorial capital region has a fiber network (Goggin et al., 2012). Usually, the company offers fixed-line telephone, fax, Internet, data, portable post-paid, mobile roaming, portable internet, fixed wireless broadband (Aironet), Evolution-Data Optimized (EVDO), fixed broadband Asymmetric Digital Subscriber Line (ADSL), a virtual private network (VPN), videoconference and Teleconferencing (Goggin et al., 2012).

Among them, fixed-line telephone and fixed wireless broadband (Aironet) administrations have a long history in Ethiopia. Like most nations, the telecommunication network structure of Ethio-telecom has four layers, to be specific: service layer, control /aggregates layer, core /transport layer, and finally access layer. Each layer has distinctive work and contains different network equipment's (Goggin et al., 2012). Access layer is a layer that contains network elements (NEs) that can support end users (Cisco Press, 2014). These devices are usually multi-service elements so that they support customers to get different services. Access layer gives clients access the network. To supply a different kind of service, Ethio-telecom in Adama among numerous access layers device uses multi-service access gateways (MSAG) that offer assistance to put through the service provider with the client; which is set in access the layer of the integrated network structure (Core Network, 2016). Multi-service access Gateway (MSAG) A solid device of medium capacity and carrier class rolled out by ZTE, mainly develop VOIP (voice over internet protocol) service and broadband data service over the IP MAN or backbone network, and is primarily based on the existing twisted-pair line. Besides, it is appropriate to modern services that utilize conventional carrier cable resources to realize the accessing of broadband (as the second line for home clients), the getting to of ADSL or VDSL to realize the voice and data service at the same time. Moreover, it can access the corporate clients like enterprises by deploying the internal LAN to supply IP phone service (Core Network, 2016) (Rediciati Group, 2018).

Ethio-telecom holds an assortment of telecom devices that needs a reliable power source to be operational. The company got this power mainly from the national grid, and uses this power source alone or with generators and/or batteries as reinforcement. The MSAG is usually provided from a rectified 120V with a 45A supply from the main 380v AC source. When the power goes off the diesel generator can supply the device. However, this creates carbon emissions to the environment. Fossil fuels have been started to be gradually depleted. Today, most of the research is focused on the effective utilization of non-conventional energy sources. Renewable energy sources are considered as a perfect option for generating clean and sustainable energy (I. Sefa et al., 2015). Of all the existing non-conventional sources of energy, solar Photovoltaic (PV) technology is popularly used as it has many advantages with less carbon emissions. Especially solar power system finds extensive application in remote areas where access to the grid supply is impractical.

The benefits of solar Photovoltaic panel are: it absorbs the everlasting solar energy at free of cost and it is eco-friendly without generating any kind of pollution into the atmosphere and offers low noise and low maintenance, when compared with conventional energy sources. It directly converts the solar energy from Sun into DC electric power (I. Sefa et al., 2017) (M. Demirtas et al., 2015). In this research work the solar power design for the MSAG for Bole sub city in Adama is done. In addition, the DC-DC converter and the battery charge controller has been done. The system is simulated in the MATLAB/Simulink environment. For the coast analysis of the solar energy the HOMOR software is used.

1.2. Statement of the Problem

Due to the unreliability of distribution lines, national grid load shading, and long duration interruption of the main AC supply usually the MSAGs are not give service to the customer regularly. These days, specifically in Bole sub city, Adama the main grid supply goes off regularly in a week and the telecom services are not give services to the clients. Conventionally, diesel generators can be used for suppling the MSAG. However, Supplying the demand with diesel generator as a standalone is environmentally negative, noisy, and costly because of fuel and needs skilled engineers for maintenance. Moreover, the depletion rate of the fossil fuel is highly increasing all over the world.

Developing countries like Ethiopia have serious energy crisis. Satisfying the power demand of the people for the fundamental necessities by itself is in much a bother situation. Hence, governments and peoples started looking towards permanent and never-ending sources of energy called renewable energy such as solar, biomass, and wind energies. The positive aspect of use of renewable energy sources in these countries is that they are available in plenty and also pollution free. In this thesis work based on the maximum load profile of the MSAG, the solar power design including the DC - DC converter, charge controller, and battery design is implemented through mathematical analysis and MATLAB Software tool.

1.3. Objectives of the Study

1.3.1. General Objective

The main objective of this research work is to design and analyze a solar power energy for Ethio- telecom multi-service access gateway (MSAG) device.

1.3.2. Specific Objectives

The specific objectives of this research thesis are:

- To analyze the maximum load of the MSAG.
- To model the selected PV module.
- To model appropriate DC-DC converter and P&O MPPT technique.

- To simulate the system’s operation with MATLAB and HOMER softwares.
- To make conclusions and recommendations based on the results of the simulation.

1.4. Scope of the Study

The scope of this research work is designing solar powered multi-service access gateway (MSAG) system mathematically and analyzing optimizing the required data through MATLAB simulation and HOMOR softwares.

1.5. Limitations of the Study

The thesis is limited to the simulation of the system using MATLAB/Simulink by showing how the different components of the system interact with each other. The reason behind this is the implementation of a real system, which is difficult to procure the components and cost incurred in making the actual implementation.

1.6. Motivation of the Study

In Ethiopia, the communication technologies have been increasing widely. The wired cellphones and ethernets are familiar with Ethiopian people, government, and in the private sector offices. These are supplied from Multi-Service Access Gateway (MSAG). A MSAG is getting power supply from the national grid. Even though, the country is building and constructing different energy resources, sometimes the power may off. At the time the MSAG is not suppling the communication data to the customer. This leads to further investigation and research development for having additional environment friendly energy sources. Hence, solar power plants are emission free and has less investment cost as compared to the hydropower plant and other energy resources.

1.7. Significance of the Study

The significance of this study is to ensure service continuity and reduce dependency on commercial line of Ethiopian Electric Utility (EEU) through an optimal sizing of standalone PV system. In addition, the research shows that, the availability of alternative PV power source for Ethio-telecom access layer devices and to minimize the power cost. Furthermore, this research encourages further studies that can be done to utilize available alternative power sources for other network equipment's.

1.8. Thesis Organization

This research thesis comprises five chapters.

Chapter 1: Presents introduction of the research work, statement of the problem, research questions, objectives, scope, limitation, motivation and significance of the research thesis.

Chapter 2: Describes the theoretical background of the PV system and review of the related works in the area of the study.

Chapter 3: Provides the methodologies followed in this research thesis.

Chapter 4: Presents the proposed results and discussions.

Chapter 5: Discusses conclusion and recommendations.

CHAPTER TWO

THEORETICAL BACKGROUND AND RELATED WORKS

2.1. Chapter Overview

This chapter discusses on the overall theoretical background and concept of the proposed study area in general. It includes the background of renewable energies, solar energy, MSAG, and finally related works to the proposed study. Moreover, this chapter will show the theory and concept used to solve the problem. Theoretical understanding is very important as a guide in doing any kind of research.

2.2. Renewable Energy

In spite of the fact that, fossil fuels are still widely used at the cutting-edge day, they are being gone through by mankind much faster than they are replaced by natural resources. As a result, fossil fuels are regarded as being non-renewable at the current rate of utilization. Recent research has shown that the request for renewable sources of energy is an issue of essential concern at the present moment (L. Tolbert et al., 2015) (J. Malla et al., 2018).

Currently, the renewable resources of energy are responsible for around 13.6% of the world's energy usage. Furthermore, by the year 2040, the contribution of renewable energy sources to worldwide energy utilization is anticipated to be around 47.7% (EEP, 2016). One of the foremost noteworthy advantages of renewable sources of energy is their input within the lessening of environmental pollution and its possible elimination on an enormous scale (H. Mark, 2010).

2.2.1. Renewable Energy Scenario in Ethiopia

Ethiopia has a huge amount of renewable energy resources and has the capacity to generate over 60GW of electric power from hydroelectric, wind, sun-powered, and geothermal sources (EEP, 2016). The need for electricity has been relentlessly expanding due to Ethiopia's fast GDP growth over the past decade. The country is encountering energy shortages as it struggles to meet developing electricity demand which is forecast to grow by approximately 30% per year in spite of Ethiopia's huge energy potential. Table 2.1 shows the energy resource potential of Ethiopia.

Table 2.1 Energy resource potential of Ethiopia (EEP, 2016)

Resource	Unit	Exploitable Reserve	Exploited Percent
Hydropower	MW	45,000	<5%
Solar/day	kWh/m^2	4 – 6	<1%
Wind: Power Speed	GW m/s	100 >7	<1%
Geothermal	MW	<10,000	<1%
Wood	Million tons	1120	50%
Agricultural waste	Million tons	15-20	30%
Natural Gas	Billion m^3	113	0%
Coal	Million tons	300	0%
Oil shale	Million tons	253	0%

Source: Ethiopian electrical power (December 2016)

2.2.2. Solar Energy in Ethiopia

Solar power has got a powerful potential of energy that can be harnessed using a variety of devices. With the added advantage of minimum maintenance, solar energy systems are easily available for industrial and household use with recent advancements (V. Quaschnin, 2010). The estimated national yearly average irradiance is to be 5.2 kWh/m^2/day with seasonal variations that range between the minimum of 4.5 kWh/m^2/day in July to a maximum of 5.6 kWh/m^2/day in February and March. The solar resource is moderately lower within the most crowded Northern, Central, and Western highlands of the country whereas the rift valley regions, Western and Eastern lowlands of the country get higher yearly average irradiance well over 6 kWh/m^2/day.

2.3. Standard Test Conditions

The comparison between distinctive photovoltaic cells can be done on the basis of their performance and characteristic curve. The parameters are always given in the datasheet. The datasheet makes available the notable parameter regarding the characteristics and performance of PV cells with respect to the standard test conditions (Metrology, 2020). Standard test conditions are irradiance at 1000[w/m], temperature at 25 ^oC, and Spectrum x at 1.5 i.e., AM1.5.

2.4. Photovoltaic System Arrangement

The PV manufacturers use crystalline silicon thin film technologies to make modules. Single crystal silicon (single-Si), polycrystalline silicon (poly- Si) wafers are made into solar cells in the former (J. Lee et al., 2006) (Panels, 2020). The cells are assembled in to modules by solar cell manufacturers. A typical crystalline silicon module consists of a series circuit of 72 cells, encapsulated in a glass and plastic package for prevention from the environment. Typical conversion of solar energy to electrical energy efficiencies for common crystalline silicon modules are in the 11 to 15% range (J. Lee et al., 2006) (Panels, 2020). Figure 2.1 shows the arrangement of photovoltaic system.

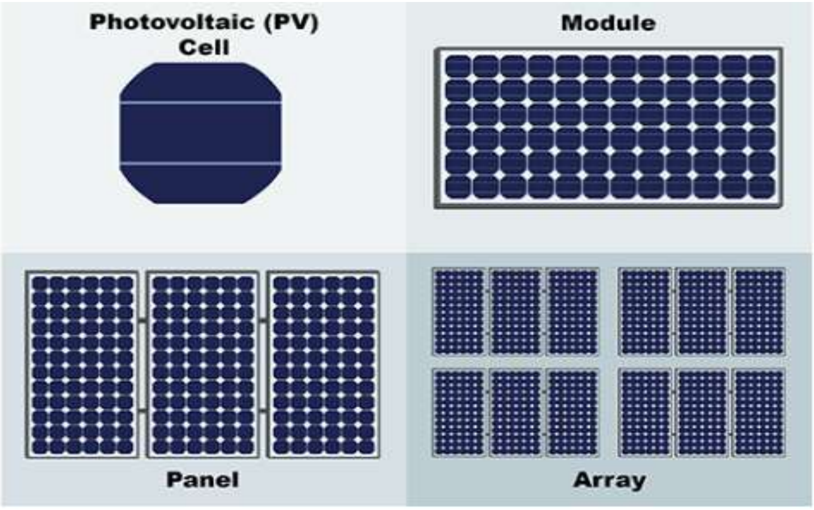

Figure 2.1 Photovoltaic cells, modules, panels and arrays (J. Lee et al., 2006)

2.5. Factors that Affect Reliability and Performance of PV Cell

2.5.1. Solar Cell Conversion Efficiency (η)

The proficiency of a PV solar cell is the proportion of the generated most extreme yield power to the incident or input power (M. Martino, 2012). A few of the output parameters influence how efficient a solar PV cell is and they are characterized as follows.

$$\eta = \frac{V_{oc} \times I_{sc} \times FF}{P_{in}} \tag{2.1}$$

where: V_{oc} = Open circuit voltage, I_{sc} = the short circuit current, P_{in} = the incident light power on the device, and FF = the fill factor.

2.5.2. Short Circuit Current

The short-circuit current is the current found when the negative and positive terminals of the cell are short-circuited; moreover, the voltage between the negative and positive terminals is zero, which corresponds with zero load resistance (M. Martino, 2012). It depends on the spectrum of the incident light and incident photon flux density.

2.5.3. Open Circuit Voltage

The open-circuit voltage is the maximum voltage in absence of current flows through the external circuit. In open-circuit voltage, the solar PV cell terminals are opened or disconnected from a load. It is the maximum voltage that a photovoltaic solar cell can deliver under any illumination.

2.5.4. Fill Factor

Fill factor (FF) is one of the important parameters to identify the efficiency of the solar photovoltaic module. To provide the maximum efficiency, the fill factor must be maximum and approach to unity on the current versus voltage curve of the solar photovoltaic module. However, the fill factor value gives an idea of the quality of the PV array, and the closer to unity the more power the array can provide (D. K. Sharma, 2014).

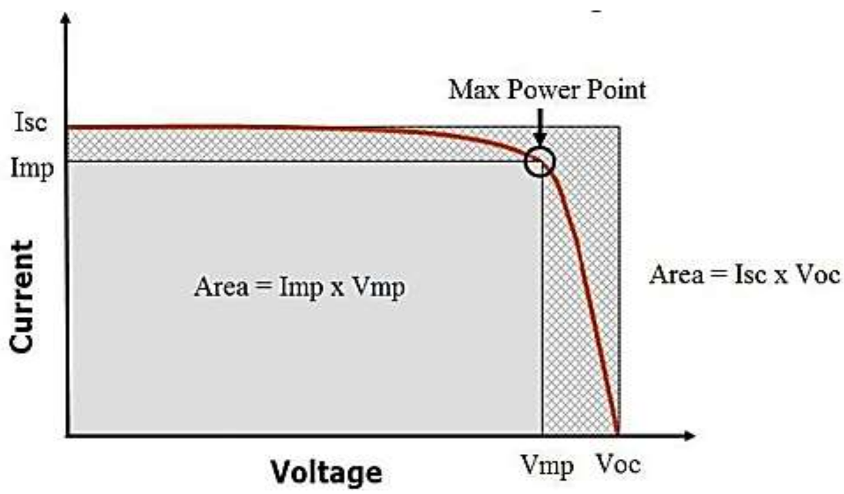

Figure 2.2 I-V Curve with a varying fill factor of solar cell (D. K. Sharma, 2014).

Because of the existence of parasitic elements in the photovoltaic cell, the value of FF decreases. Due to this, the values of the fill factor are between 0.7 and 0.8. It is the ratio of theoretical power to the maximum power and mathematically expressed as follows. I-V Curve with a varying fill factor of solar cell is shown in Figure 2.2.

$$FF = \frac{V_{mp} \ I_{mp}}{V_{oc} \ I_{sc}} \quad (2.2)$$

2.6. Photovoltaic System

There are different types of PV systems that are available. These systems are categorized by the main categories of standalone system, grid connected, and hybrid system.

2.7. Energy storage systems

PV power generation varies with the amount of sunlight shining on the panels at an instance, which results in lack of power generation during night time and cloudy weather. At such times, energy storage used to control the voltage level and the power flow through a bidirectional converter (L. Yoo et al., 2014) (E. Raszmann et al., 2017). Some characteristic parameters of the battery, which apply to the DC micro grid, are the following:

2.7.1.1.Types of Electric Battery

Rechargeable batteries play an important role in our lives and many daily chores would be unthinkable without the ability to recharge (R. A. Dougal et al., 2002) (M. Rivera, 2008) (A. Nyman et al., 2012). The most common rechargeable batteries are secondary batteries which are lead-acid, NiCd, NiMH, and Li-ion. Figure 2.3 shows the classifications of all types of electric batteries.

2.7.1.2.Comparison of Electric Batteries

In general, the comparison performance of battery for PV can be summarized as shown in Figure 2.6 based on battery performance characteristics of each maximum of five points (A. Nyman et al., 2012). Lithium-ion batteries has good performance parameters than other type of batteries for PV. It has higher energy density, longer life span, and higher power density than most other practical batteries. Complicating factors include safety, durability, thermal breakdown and cost. Li-ion batteries should be used within safe temperature and voltage ranges in order to operate safely and efficiently. The graphical comparisons of different batteries are shown in Figure 2.4 respectively.

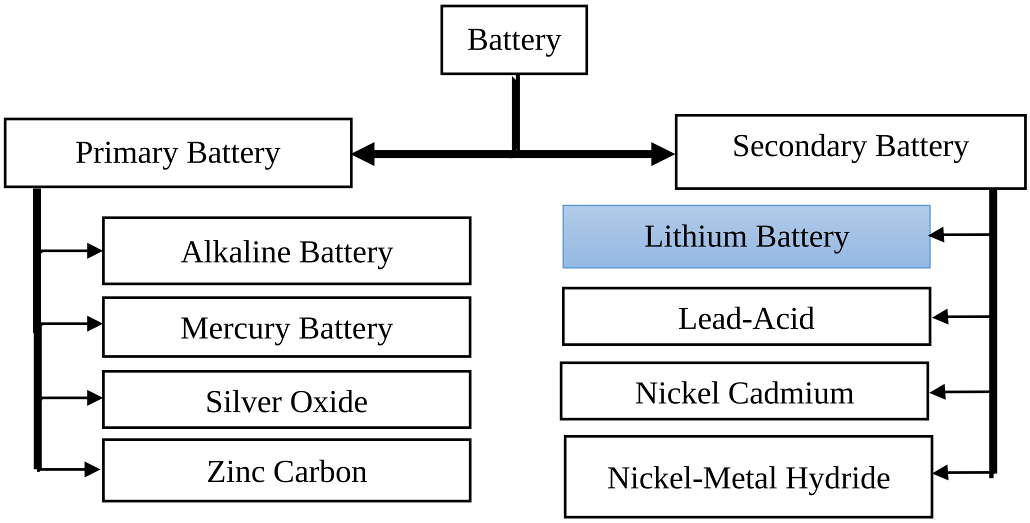

Figure 2.3 Types of electric battery (M. Rivera, 2008)

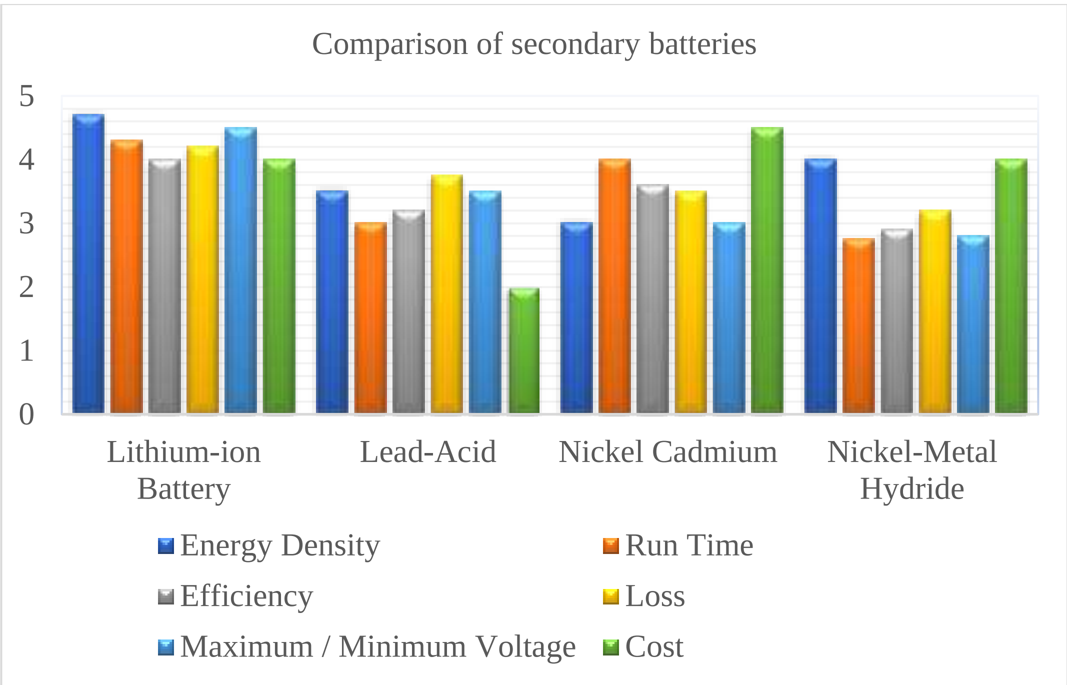

Figure 2.4 comparison of secondary batteries (Lu L et al., 2012)

2.8. Theoretical Background of MSAG

As of now, Ethio-telecom is the sole service provider of telecom technology in the whole nation with comprehensive plans in place to meet the necessities set out by the Ministry of Counsels. Ethiopia owned and controlled all telecommunications services, but an offering of Client Premises Equipment (CPE) (Baron et al., 2010). Information Communication

Technology (ICT) infrastructure that gives a blended coverage of 80% of the country's population, with the potential to serve 90% of its population. Over 700 cities have been connected to fixed-line Internet and each regional capital municipality has a fiber network. Network architecture of Ethio telecom has four layers, specifically: service layer, control /aggregates layer, core /transport layer and finally access layer (Goggin, G, 2012).

2.8.1. Network Evolution of MSAG

The access layer is a layer that contains network elements (NEs) that can support consumers (Cisco Press, 2014). They can incorporate routers, switches, bridges, shared-media centers, and remote access points (Cisco Press, 2014) (Salih T et al., 2014). Aggregation layer, as its name indicate, aggregates the access layer network element to the core network (Core Networking, 2016) (Radicati Group, 2018) (Priscilla O, 2012). To provide a different kind of service, Ethio-telecom in Adama among numerous access layer devices uses MSAG that offer assistance to put through the service provider with the client; which is set in the access layer of the integrated network structure as shown in Figure 2.5.

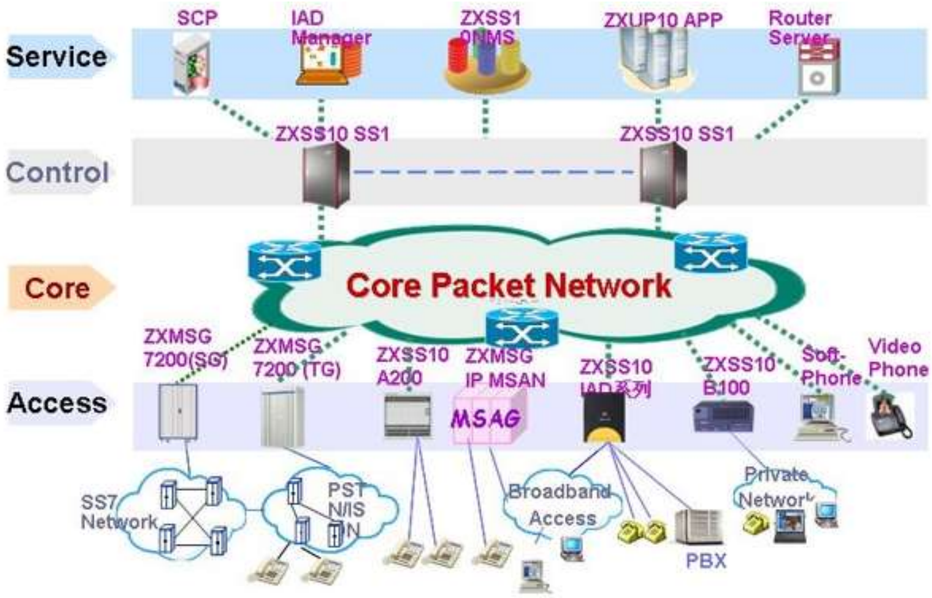

Figure 2.5 Internal architecture of the MSAG (Priscilla O, 2012).

Multi-service Access Gateway (MSAG) a solid device of medium capacity and carrier-class rolled out by ZTE, basically develop VOIP (voice over internet protocol) service and broadband data service over the IP MAN or backbone network, and is essentially based on the existing twisted-pair line or BRI interfusing at accessing side. Furthermore, it is suitable for new services who employ conventional carrier cable resources to realize the access of broadband (as the second line for home clients), the accessing of ADSL or VDSL to realize the voice and information service at the same time. Moreover, it can access corporate clients like enterprises by deploying the internal LAN to provide IP phone service (Core Networking, 2016) (Salih T et al., 2014).

2.8.2. Characteristics of MSAG

Interfaces: Subscriber-side, xDSL subscriber, Ethernet, GPON, Network-side, Optical interface, ATM, Maintenance serial port, Maintenance network port, Environment and power monitor port.

Functions: supporting broadband ADSL/ADSL 2+, VDSL/Ethernet, PSTN service, ISDN service, FAX ser- vice, V5 interface, xDSL service, CES service and GPON service, support real time transport protocol, support code and encode arithmetic G71, G729, supporting the two-layer switching, supporting standard protocol and incorporating first-class compatibility, supporting 256 VLANs; supporting 64 multicasts

Capacity: 2000 analog subscribers, 2000 ADSL subscribers, 928 VDSL subscribers, minimum 240 VOIP port. It is having high density, easier operation and matinees, outdoor service with Wight of 620kg, smaller power consumption 1050W,

2.9. Related Works

Many researchers have studied the microgrid energy management control system. Many authors have been studied based on renewable energy resources, and the results have been published. Among them, a few thesis papers are reviewed in the following section.

The modeling, designing, and analysis of a standalone PV DC microgrid system were proposed in literature (Swash W et al., 2019). The components of the system were a solar PV system, DC to DC converter, maximum power point tracking, bi-directional DC/DC converter, batteries, charge controllers, and DC-AC inverter. Fuzzy logic with MPPT control was used to control the maximum power. Moreover, bi-directional converters have been implied to control the battery charging and discharging system.

The author in (M. B. Kumar, 2017) investigated the modeling, designing, and analysis of a standalone PV, DC microgrid system. As the PV power system is increasing widely around the glob, the carbon emission will be reduced to some extent especially by replacing the deasil generators. As a result, the author was motivated by increasing concern about global warming, the upsurge of gas prices, and the pollution of petroleum energy.

Energy management control for stand alone PV in a remote area were investigated in (Abhishek K et al., 2017) to employ electric access. The modeling of the system was developed in MATLAB, and for the optimization and integration HOMER Pro software was used. The results obtained were to manage the energy flow from source to load was cost-effective and reliable. The study did not discuss the bidirectional converter to stabilize the system.

In a similar fashion, a control and energy management strategy of standalone PV and battery storage management were studied in (H. M. Mohammad, 2018). In this study, the operation of PV and the behavior of energy storage system at different operating conditions (solar radiation and temperature changes) were evaluated. The DC transformers with PI control algorithms were investigated to control the system performance and load power balancing. The PV bus voltage level is employed as an information carrier for the controller to maintain stability and improve efficiency. In this study, the difficulty is the incremental conductance algorithm is reaching slowly at the maximum power for high change of irradiance which leads to disturbance of power. To overcome this problem, P&O algorithm is better than incremental conductance algorithm to truck the maximum power point with in a very short period of time.

The author in (M.K Pooja et al., 2020), proposed the bidirectional DC to DC converter for solar battery backup applications were presented. The solar photovoltaic-based system with energy storage with the help of a bidirectional DC to DC converter was accomplished in this proposed work. By using PI controllers, the output across the load is maintained with controlled input. The simulation is carried out using MATLAB/Simulink.

The design and simulation of a stand-alone PV power plant for a small island in Belize were developed in literature (J. Grant, 2018). The study was used MATLAB/Simulink to simulate all components of the system. For the design of the system PV modules, MPPT, bidirectional DC-DC converter, battery, and battery management system were considered. Also, a financial analysis was conducted using the HOMER software.

In general, form the above related works the modeling and design of stand-alone and grid connected PV was modeled through different techniques. The modeling was including the design of the dc-dc converters and the battery management system. Most of the study were conducted for only considering the rural areas only. However, there are also many things that the researchers should think in the urban area especially for the public service areas. In this research work, the design of stand-alone PV with battery management system is proposed and developed for the Mult-service Access Getway (MSAG) in Ethio-telecom application. In doing this, the cascade PID controller was used for the control of the MPPT based on the P&O algorithm and the battery management system.

CHAPTER THREE

METHODOLOGY

3.1. Introduction

This chapter deals with the data collection, designing process of mathematical modelling for photovoltaic cell, designing and modelling of buck converter, modeling back-to-back converter, battery sizing, and the proposed PV system energy cost analysis.

3.2. Materials

For the system design and editing thesis documentation the following computer softwares are used.

- Microsoft office 2019,
- MathType 6.0 equation,
- MATLAB/2019a, and
- HOMER Beta software.

Microsoft office is used for editing the thesis documentation. MathType 6.0 is used for writing mathematical equations in Microsoft office word and Power point presentation tools. MATLAB is used for simulation of the system design. HOMER Beta software is used for cost analysis of the proposed system.

3.3. Methods

In order to attain the above general and specific objectives of the thesis, the following methods and techniques is followed. First the related works are reviewed and then, the necessary data are collected and analyzed. After that, the load demand of the system is determined and PV module is designed based on the load demand. The DC-DC buck converter is designed to get the required output voltage. Finally, the proposed system is developed by using MATLAB/Simulink and the result is discussed and conclusion is drawn. Figure 3.1 shows the block diagram of the research methodology.

3.4. Block Diagram of the Proposed System

The proposed system mainly consists PV array, MPPT, DC-DC converter, charge controller, and battery sizing. In this thesis PV array is used to generate the DC power from the solar energy and MPPT is incorporated with it to track the maximum power. Then the output voltage of the PV array is stepped down by using the DC transformer so called buck converter. To get stable and smooth response, the output voltage of the buck converter is controlled by using convectional PID controller. The battery charge controller is controlled using the bi-directional DC-DC converter and the PID controller.

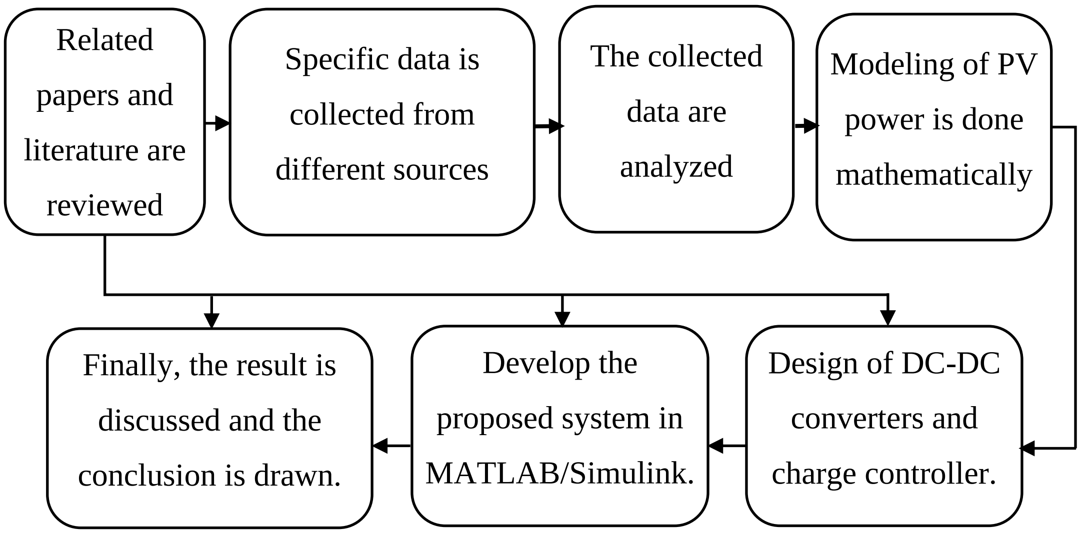

Figure 3.1 Block diagram of the proposed methodology

The overall completed solar powered based Multi-service Access Getway (MSAG) with battery design for Ethio-telecom is designed. The layout of the proposed system is shown in Figure 3.2.

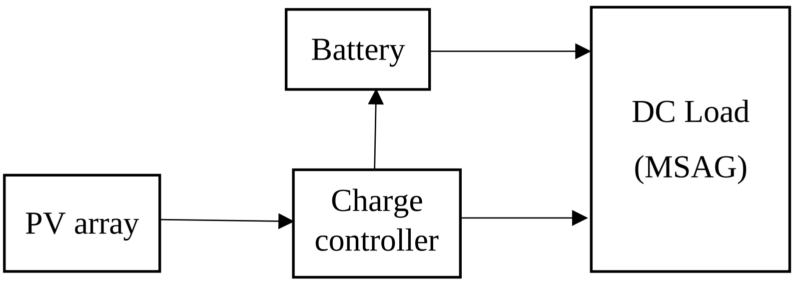

Figure 3.2 The layout of proposed system

3.5. Sunshine Per Hour Data of Metrology

Adama is one of the Oromia region's cities in Ethiopia which is located 99km from Addis Ababa. It is found at latitude 8.54^0 N and longitude 39.27^0 E at an elevation of 1712m that is taken from NASA. The following Figure 3.3 shows Adama city on Google map.

Figure 3.3 Adama city, Eastern Shewa, Ethiopia

Source: Google map

Table 3.1 shows sunshine/hour data of the selected area taken different consecutive years.

Table 3.1 Sunshine per hour data of the selected area

Year	Jan	Feb	Ma	Apr	May	Jun	Jul	Aug	Sep	Oct	Nov	Dec
2013	8.9	10.1	8.5	8.1	8.4	7.9	5.3	6.9	8.4	8.3	8.8.	10.1
2014	9.5	8.7	8.6	9	8.7	8.7	6.4	6.9	6.6	8.8	9.4	9.7
2015	9.8	10.1	9.6	8.8	7.7	7.6	9.4	8	8.4	9	9.1	8.9
2016	7.7	8.9	9.4	6.7	6.2	7.9	6.5	6.8	7.2	9.9	9.1	9.8
2017	9.9	9	9.3	9.6	7.9	8	6.2	6	6.8	8.7	10	9.4
Ave	9.16	9.36	9.08	8.44	7.78	8.02	6.76	6.92	7.48	8.94	9.4	9.58

The graphical data of annual average monthly sunshine is shown in the Figure 3.4 below.

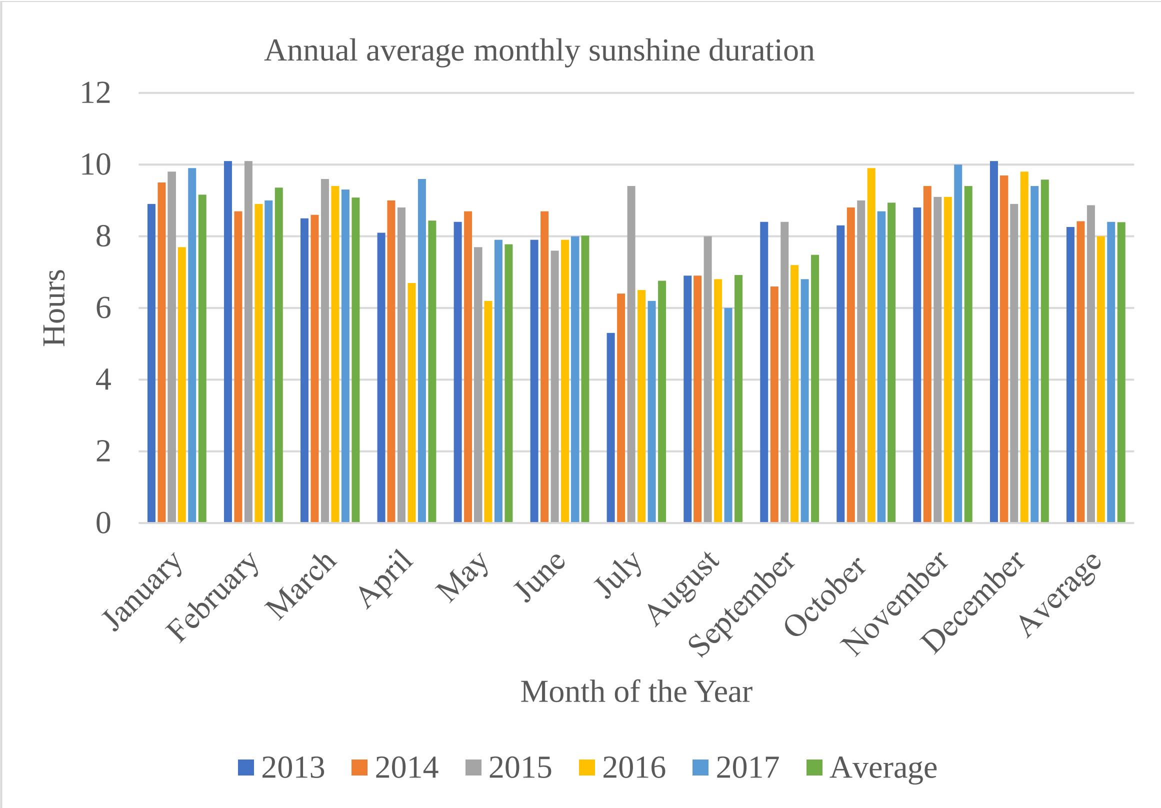

Figure 3.4 Graphical representation of annual average monthly sunshine duration

Form (Berket Fola, 2020) and form the NASA sunshine data, the following result is found for comparison. Table 3.2 shows the solar radiation from different sources.

Table 3.2 Solar radiation from different sources

Month	H(Calculated)MJ/m^2	NASA		Month	H(Calculated)MJ/m^2	NASA
Jan	5.84	5.909		Jul	5.86	5.568
Feb	6.38	5.930		Aug	6.04	5.641
Mar	6.73	6.256		Sept	6.20	5.983
Apr	6.66	5.928		Oct	6.30	6.348
May	6.36	6.444		Nov	6.01	6.321
Jun	6.35	6.247		Dec	5.80	5.941

As it is observed from the above table, the solar radiation value from NASA and calculated is almost similar. For this purpose, the value of solar radiation which is found from the NASA is used as the input for the software and PV design. Figure 3.5 shows the graphical representation of solar radiation of different sources.

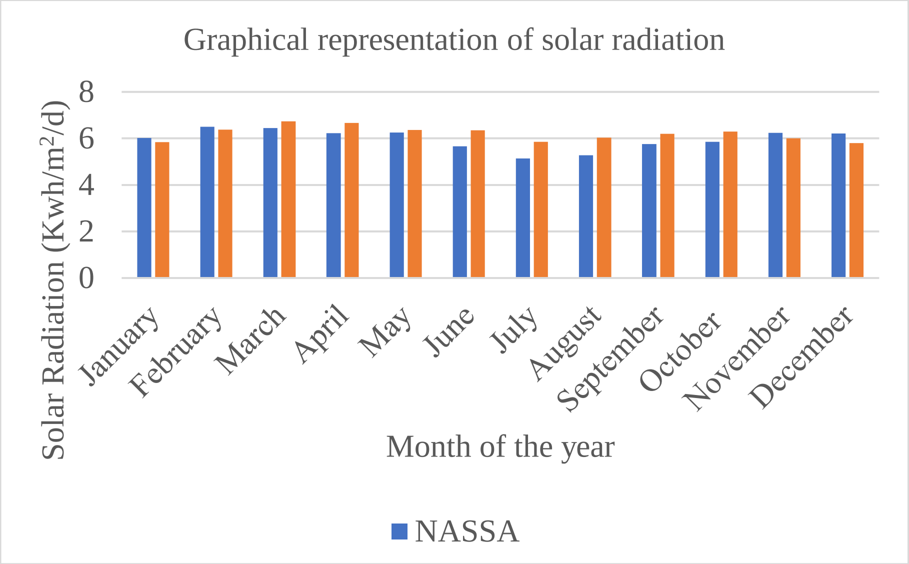

Figure 3.5 Graphical representation of solar radiation

3.6. Energy Demand and Load Estimation

The MSAG has contained two types of loads such as DC power supplies and fan motor for the cooling of the power supply controller. They are shown in the following Table 3.3.

Table 3.3 MSAG load demand and estimation

Location and type of loads	Quantity	Rating (W)	Adjusted Power (W)	Hrs./day	Energy/day (kWh/day)
Power supply-1	1	720	720	24	17.28
Power supply-2	1	720	720	24	17.28
Power supply-3	1	720	720	24	17.28
Fan	1	1900	1900	15	28.5
Total loads			Total watt = 4.06kW		Total energy = 80.34kWh

The above Table 3.3 describes all the equipments in the MSAG with their energy consumption and operating quantity. And also, the total energy consumption of the electrical service for the MSAG was described for each appliance. And, the energy capacity of the total load is 80.34kWh.

3.6.1. Mathematical Modeling of the Photovoltaic

A photovoltaic system converts sunlight into electricity, where, the basic device of a photovoltaic system is the photovoltaic cell. Cells may be grouped to form panels or modules. The modelling of photovoltaic (PV) has made a great transition and form an important part of power generation in this present age. The modelling of PV module generally involves the approximation of the non-linear (I-V) curves.

Many researchers used circuit-based approach to characterize the PV module of which the simplest model is the current source in parallel to a diode. The circuit models for photovoltaic cell are listed below.

3.6.1.1. Ideal Photovoltaic Model

An ideal Photovoltaic cell consists of a single diode connected in parallel with a light generated current source, I_{ph} as shown in the figure below, were, its output current, I, can be written as:

$$I = I_{ph} - I_s \left[\exp\left(\frac{V}{nV_T} \right) - 1 \right] \tag{3.1}$$

where, I_s is cell saturation of dark current, V_T is thermal voltage ($V_T = {KT_C}/{q}$), K is Boltzmann's constant (1.38*10−23 J/K), T_C is cell's working temperature, Q is electron charge (1.6* 10−19 C), and n is ideality factor equal to 1.1. The ideal photovoltaic model is shown in the Figure 3.6 below (I. Kashif et al., 2011).

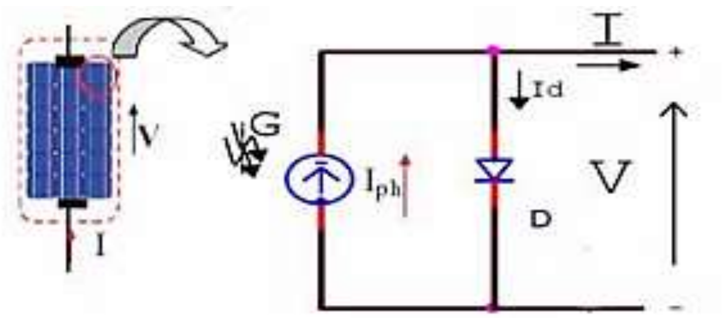

Figure 3.6 Ideal photovoltaic model (I. Kashif et al., 2011)

3.6.1.2. Non-Ideal Photovoltaic Models

The photovoltaic model with series resistance (Rs-model) depicted in Figure below is achieved with inclusion of series resistance Rs, hence, the output current can be derived as (I. Kashif et al., 2011) (J. Abdul et al., 2012):

$$I = I_{ph} - I_s\left[\exp\left(\frac{V + IR_s}{nV_T}\right) - 1\right] \tag{3.2}$$

The photovoltaic model with series resistance is shown in Figure 3.7 below.

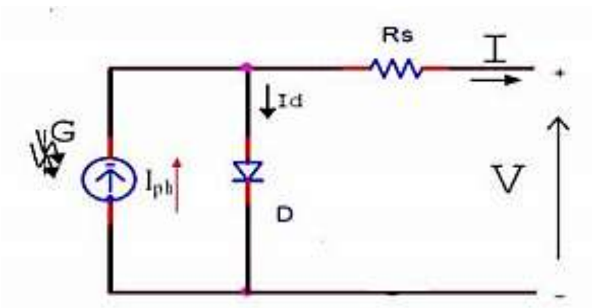

Figure 3.7 Photovoltaic model with series resistance (I. Kashif et al., 2011)

The above equation does not adequately represent the behavior of the cell when subjected to environmental variations, especially at low voltages. A more practical model can be seen in Figure below, where series Rs, and parallel resistances R_{sh}**,** are introduced (I. Kashif et al., 2011) (J. Abdul et al., 2012). Series resistance is very small, which arises from the ohmic contact between metal and semiconductor internal resistance. But shunt resistance is very large and represents the surface quality along the periphery, noting that in ideal case R_s is 0 and R_{sh} is ∞ (I. Kashif et al., 2011) (J. Abdul et al., 2012). Applying Kirchhoff's law to the node where I_{ph}, diode, R_{sh} and R_s meet, and one get:

$$I = I_{ph} - I_d - I_{sh} \tag{3.3}$$

$$I = I_{ph} - I_s\left[\exp\left(\frac{V + IR_s}{nV_T}\right) - 1\right] - \left[\frac{V + IR_s}{R_{sh}}\right] \tag{3.4}$$

where I_d is diode current, G is solar insolation, I_{sh} is shunt current.

This model yields more accurate results than the R_s model, but at the expense of longer computational time. A modification of this model was proposed by several authors by adding an extra diode. This additional diode represents the recombination effects of the charge carriers. In general, the two-diode model is more accurate but the computational time is much longer (I. Kashif et al., 2011) (J. Abdul et al., 2012).

For simplicity, the single diode model of Figure below was used throughout the present work. The photovoltaic model with series and parallel resistance is shown in Figure 3.8 below.

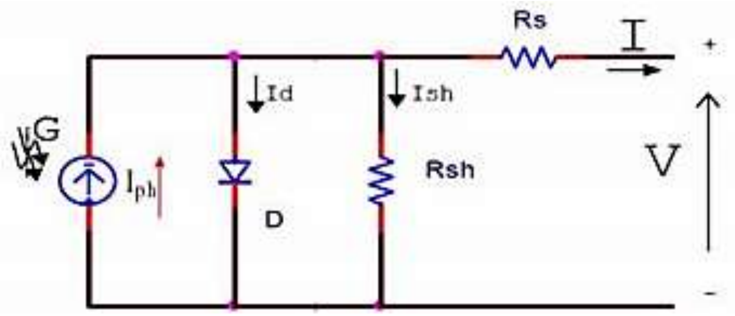

Figure 3.8 Photovoltaic model with series and parallel resistance (I. Kashif et al., 2011)

The photocurrent mainly depends on the solar insolation and cell's working temperature, which is described as:

$$I_{ph} = \left[I_{scr} + K_i \left(T_c - T_{ref} \right) \right] \frac{G}{G_{ref}} \tag{3.5}$$

where: I_{scr}: solar cell short-circuits current, G_{ref} = reference solar insolation in W/m^2, T_{ref} = cell's reference temperature, K_i: cell's short-circuit current temperature coefficient, G: solar insolation in W/m^2

On the other hand, the cell's saturation current varies with the cell temperature, which is described as:

$$I_S = I_{RS} \left(\frac{T_c}{T_{ref}} \right)^3 \exp\left[\frac{qE_g}{nK} \left(\frac{1}{T_{ref}} - \frac{1}{T_c} \right) \right] \tag{3.6}$$

where, I_{RS} is cell's reverse saturation current, E_g is band-gap energy of the Si solar cell (1.10 eV), and n is dependent on PV technology.

The reverse saturation current at reference temperature can be approximately obtained as:

$$I_{RS} = \frac{I_{sc}}{\exp\left(\frac{qV_{oc}}{nKT_c} \right) - 1} \tag{3.7}$$

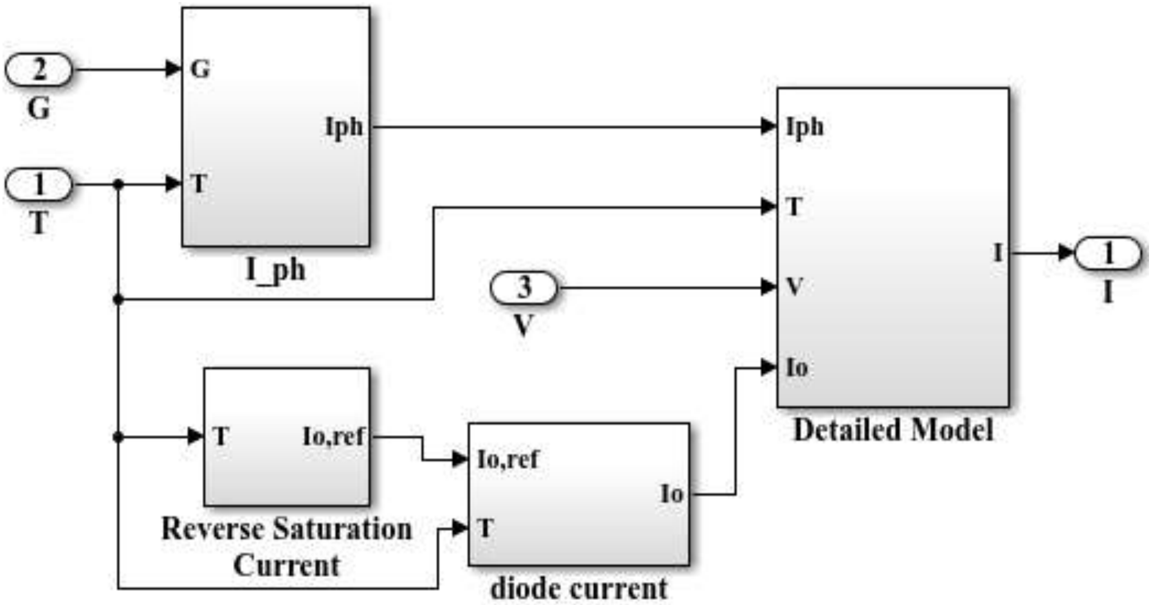

Figure 3.9 Block representation of PV module

Based on mathematical equations of the photovoltaic cells, a model was written for MATLAB software package applications. A MATLAB/Simulink has been developed which calculates the current module from data of voltage, solar radiation, and temperature. From which, the (I-V) and (P-V), as well as, maximum power point could be obtained. The overall MATLAB block implementation of the PV Module is shown in Figure 3.9.

3.6.1.3. Characteristics of Photovoltaic Cell

Photovoltaic cells generally demonstrate a nonlinear I-V and P-V characteristics which vary with the solar irradiation and cell temperature. The most important fundamental parameters used for characterizing the photovoltaic cell are: short circuit current I_{sc}, open circuit voltage V_{oc}, Maximum Power Point (MPP), efficiency (η) and Fill Factor (FF) (J. Abdul et al., 2012) (T. Huan-Liang et al., 2008).

Short Circuit Current: It is the current that reduces the effect of impedance in the circuit. When the cell is short-circuited, negligible current flows in the diode. It is calculated when V=0. However, it is largest amount current produced from the PV cell due to the photon excitation.

$$I_{ph(V=0)} = I_{sc} \quad (3.8)$$

Open Circuit Voltage: It is voltage which is not connected to any load in a circuit and no current passing through the cell. It is calculated when the voltage is equal to zero. Moreover, it is the maximum voltage difference across the PV cell when I=0. Mathematically,

$$V_{OC} = \frac{AKT}{q}\ln\left(\frac{I_{ph}}{I_s}+1\right) = V_{th} * \ln\left(\frac{I_{ph}}{I_s}+1\right) \tag{3.9}$$

where: Vth: the thermal voltage, T: operating temperature of the PV cell.

Maximum Power Point: It is the operating point where the power is maximum across the load. Mathematically (J. Abdul et al., 2012) (T. Huan-Liang et al., 2008).,

$$P_m = V_m * I_m = \alpha V_{OC} * I_{SC} \tag{3.10}$$

where: α is the fill factor.

Efficiency: It is defined as the ratio of maximum power to the incident light power. Mathematically,

$$\eta = \left(\frac{P_m}{P_{in}}\right)*100 = \left(\frac{V_m * I_m}{P_{in}}\right)*100 \tag{3.11}$$

Fill Factor: Fill Factor which is abbreviated by FF, is a parameter defined as the ratio of the maximum power from the solar cell to the product of I_{sc} and V_{oc}, expressed as (J. Abdul et al., 2012) (T. Huan-Liang et al., 2008).:

$$FF = \frac{P_{max}}{V_{OC} I_{SC}} \tag{3.12}$$

Typically fill factors ranges are from 0.5 to 0.82. Its value is more than 0.7 for good PV cells. The fill factor decreases with the increase of cell temperature.

3.7. Sizing of Standalone PV Systems and Procedures

The first step to start the sizing of the standalone photovoltaic system is to determine the load consumption that is to serve. Consequently, load estimations have been done based on the information taken from the Ethio-telecom Adama branch. To sizing standalone solar photovoltaic systems, the main points that must be estimated first were:

- MSAG load estimation,

- Sizing of the PV array and specification
- Sizing of the battery and its charge controller,
- Sizing of the DC-to-DC converter.
- Sizing of system cable and economic analysis

The following constant parameters are taken in to considerations for design and sizing the photovoltaic system. Their values are shown in Table 3.4.

Table 3.4 Constant parameters used in photovoltaic array sizing.

No.	Description	Values
1	Battery efficiency	$0.8 < x < 0.85$
2	Temperature losses	0.9
3	Wire losses	0.9
5	Depth of charge	0.65

Form Table 3.4 the combined efficiency and the output efficiency are determined as follows,

- Combined efficiency = 0.85*0.9*0.9= 0.69.
- Output efficiency, η_{out} = 0.85*0.9 = 0.765.

3.7.1. Sizing of the PV Array

Before sizing the PV array, the average energy demand in Watt-hour per day is obtained by estimating all appliances and how many hours they use each day (J. Bouori et al., 2016). The steps for sizing were as follows:

Calculate total Watt-hours per day for each appliance used: Add the Watt-hours required for all appliances to get total watt-hours per day.

Calculate total Watt-hours per day needed from the PV modules: Multiply the total appliances watt-hours per day times 1.2 to get the total watt-hours per day which must be provided by the panels. where 1.2 is the correct factor for energy lost in the system.

Calculate the total Watt-peak rating needed for PV modules: Divide the total Watt-hours per day required from the PV modules by average solar radiation to get the total peak power (H. Radu et al., 2019). The total peak power is then divided by the selected system DC voltage to get the total DC. Lastly, the number of parallel and series modules can then be determined by the following formula.

$$\text{Total DC current} = \frac{\text{Peak power}}{\text{system DC voltage}} \quad (3.13)$$

$$\text{Number of series modules } (N_s) = \frac{\text{System DC voltage}}{\text{module rated voltage}} \quad (3.14)$$

$$\text{Number of parallel modules } (N_p) = \frac{\text{Whole module current}}{\text{Rated current of one module}} \quad (3.15)$$

$$\text{The total number of modules } (N_t) = N_p \times N_s \quad (3.16)$$

Here keep in mind, in this thesis work the system DC voltage is 120V taken at the Adama city for the single MSAG. Load demand estimation of a typical multi-service access getway (MSAG) (Ed) = 80340Wh/day.

$$\text{Energy of PV } (E_{pv}) = \frac{\text{Energy demand}}{\text{Combined efficiencies}} \quad (3.17)$$

$$= \frac{80340\text{Wh/day}}{0.69} = 116{,}434.78\text{Wh/day}$$

By considering the lowest average monthly insolation which is in July minimum generation (G min) is 5568Wh/m^2/d.

Step 1: PV array sizing

$$P_{PV} = \frac{E_{pv}}{G_{min}} \times 1000\text{W/m}^2 \quad (3.18)$$

where: P_{pv} is the total power of PV array in watts, E_{pv} is the total energy required from the PV array, and G_{min} is the minimum solar radiation of a month that occurred in a year.

Therefore, using Equation (3.18)

$$P_{pv} = \frac{116{,}434.78}{5568} \times 1000 = 20{,}911.42\text{W}$$

Step 2: Load current.

$$I_{pv} = \frac{20{,}911.42\text{W}}{48} = 435.65\text{A}$$

Therefore, the PV module for design purposes Kyocera Solar KD140GX-LFBS solar panel is selected. It contains 36 poly-crystalline solar cells per module. The key specification and electrical characteristics of the given 140W cell is shown below in Table 3.5.

Step 3: Number of PV modules in Parallel (N_p) is found using Equation (3.15):

$$N_p = \frac{435.65A}{8.68A} = 50.19 \approx 51 \text{ modules (odd selection)}$$

Table 3.5 Electrical characteristics of Kyocera Solar KD140GX-LFBS module

Parameters	Values
Nominal power (P_{mpp})	140W
Voltage at nominal power (V_{mpp})	17.7V
Open-circuit voltage (V_{oc})	22.1V
Current at nominal power (I_{mpp})	7.91A
Short-circuit current (I_{sc})	8.68A
Cells per module (N_S)	36
Module Efficiency (η)	13.97%
Parallel resistance of PV model (R_P)	37.404Ω
Series resistance of PV model (R_S)	0.23219 Ω
Current temperature coefficient (α)	0.02%/ ^oC
Voltage temperature coefficient (β)	- 0.31%/ ^oC

Step 4: Number of series modules (N_s) is found using Equation (3.14):

$$N_s = \frac{48}{22.1} = 2.17 \approx 3 \text{ modules but } 3 \times 22.1 = 66.3V \text{ (bus voltage)}$$

Step 5: Total number of modules using Equation (3.16): $N_t = N_p \times N_s = 51 \times 3 = 153$ modules. Sizing of the area covered by the solar module is very necessary during the design of the PV system so, considering the PV module length and width: L= 1500mm, W = 668mm.

$$A = L \times W \tag{3.19}$$

$$A = (1500mm \times 3) \times (680mm \times 51)$$

$$A = 134{,}640{,}000mm^2 = 156.06m^2$$

3.7.2. DC-DC Converter

A buck converter is a step-down DC-DC converter consisting of inductor, capacitor, power diode, and power semiconductor switch (Shafinaz A et al., 2016).

3.7.2.1. Power Semiconductor Device

In its crudest form a switch can be a toggle switch which switches between supply voltage and ground. Here transistors chosen for use in switching power supplies must have fast switching times and should be able to withstand the voltage spikes produced by the inductor (N. Mohan et al., 2007). The most popular switching devices are SCR, GTO, IGBT, and MOSFET. Among different types of switches MOSFET and IGBT are compared on the Table 3.6. Due to its several advantages over the MOSFET, the IGBT switch is used in this research thesis.

3.7.2.2.DC-DC Boost Converter Design Procedures

When the switch in Figure 3.10 above is closed the voltage across the inductor is $V_L = V_S$. The current flowing through an inductor gradually increases and the diode will be an open circuit due to the short circuit at the switch.

When the switch is opened the source and the load are connected and the diode is forward biased and the voltage across the inductor is $V_L = V_S - V_O$ (neglecting drop across diode) across inductor. As a result, the DC source and energy stored in the inductor supplies the load and the current in the inductor starts decrease gradually. DC-DC boost converter diagram and its design for 120V (4060W) stated in this section.

Inductor selection: The filter inductor value and its peak current are determined based on the specified maximum inductor current ripple [50].

$$L = \frac{D \times (1 - D)^2 \times R}{2 \times f_s} \tag{3.20}$$

where, D = duty cycle (%), f_s = switching frequency (Hz), L = inductance (H) R = load resistance (Ω).

Table 3.6 Comparison between MOSFET and IGBT (N. Mohan et al., 2007)

MOSFET	IGBT
MOSFET is the voltage-controlled device.	IGBT is voltage-controlled device
Three terminals of the MOSFET are gate (G), drain(D) and source (S).	IGBT has also three terminals namely gate (G), drain (D) or emitter (E) and source(S) or collector (C).
The input impedance of MOSFET is very high.	Input impedance of IGBT is very high.
MOSFET has positive temperature coefficient. When compared to the IGBT, with increase in temperature on-state resistance increases.	IGBT has positive temperature coefficient. With the increase in the temperature the on-state resistance increases but rate of increment is less than increase in MOSFET.
The on-state voltage drop of the MOSFET is large when compared to voltage drop of IGBT.	IGBT has very low voltage drop.
The on-state voltage drop of the MOSFET increases by three times for the temperature rise from room temperature to 200^{0}C.	The increment of on-state voltage drop of IGBT is very small.

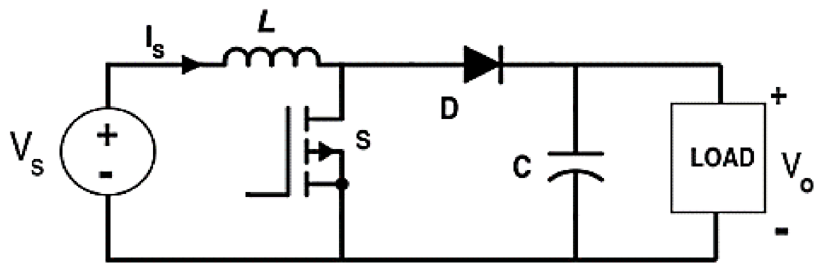

Figure 3.10 DC-DC boost converter circuit diagrams (J. Ejury, 2013)

From Table 3.3; P = 4060W, V_0 = 120V, V_S = 66.3V (bus voltage). The load resistance R can be determined form the bus voltage of the solar panel output (66.3V) and the power demand in case of when the load voltage is 120V.

$$R = \frac{V_O^2}{P} = \frac{(120V)^2}{4060W} = 3.5468\Omega$$

From the required output voltage of DC-DC converter and the bus voltage, the duty cycle can be calculated as:

$$D = 1 - \frac{V_S}{V_O} = 1 - \frac{66.3V}{120V} = 0.4475$$

Referring Equation (3.34) the inductor is calculated as follows,

$$L = \frac{04475 \times (1 - 0.4475) \times 3.5468}{2 \times 20000} = 0.02192\text{mH}$$

Capacitor Selection: The function of the capacitor is to filter the inductor current ripple and passing a stable output voltage (J. Ejury, 2013) (D. W. Hart, 2010). It also has to ensure that load steps at the output supported before the regulator is able to react.

$$C = \frac{D}{r \times R \times f_S} \tag{3.21}$$

Assume the ripple factor r is 2% of the output voltage.

$$C = \frac{0.4475}{0.02 \times 3.5468 \times 20000} = 315.4\mu\text{F}$$

From the datasheet, a capacitor having magnitude of 3000µF, and an inductor with magnitude of 4mH is selected for the buck DC-DC convertor (D. W. Hart, 2010).

3.7.2.3. Boost Convertor Voltage Control

Boost convertor is connected to the load is used to provide constant output voltage of 120v DC for the three power supplies and DC fan motor connected in parallel in the MSAG. However, due to the ON and OFF cases of the fan motor, there is a random variation of load throughout the day, the load voltage may not be constant. To maintain constant voltage, boost convertor coupled with Proportional, Integral, and Derivative (PID) controller is used. Most commercial controllers provide full PID control action (R.S. Burns, 2001).

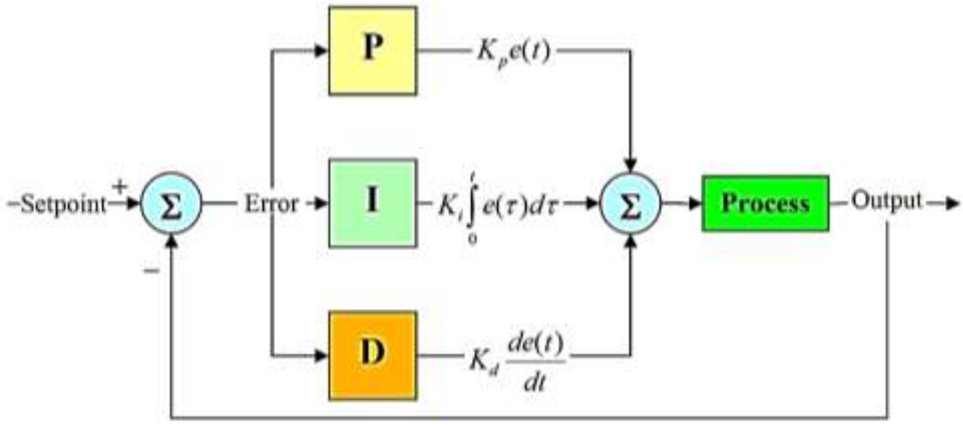

Figure 3.11 Structure of PID controller (R.S. Burns, 2001).

By tuning the three constants in the PID controller algorithm, it can provide control action designed for specific process requirements (R.S. Burns, 2001). The output of PID controller u(t), is equal to the sum of three signals. The signal obtained by multiplying the error signal by a constant proportional gain K_p, plus the signal obtained by differentiating and multiplying the error signal by constant derivative gain K_d and the signal obtained by integrating and multiplying the error signal by constant internal gain K_i. Generally, the PID controller in time domain is given as,

$$PID(t) = K_p e(t) + K_i \int e(t)dt + K_d \frac{de(t)}{dt} \tag{3.22}$$

$$PID(s) = e(s) * G_p(s) = e(s)\left[K_p(s) + \frac{K_i(s)}{s} + sK_d(s)\right] \tag{3.23}$$

Equation (3.22) written in time domain and Equation (3.23) written in Laplace's transform. The advantages of the PID controller are controlling the object, which is highly nonlinear and uncertain (R.S. Burns, 2001). After deriving the transfer function of PID controller, the next step is finding the transfer function of the buck converter. When switch is on condition, the equation for inductor current and capacitor voltage will be:

$$\frac{diL}{dt} = \frac{-Vc}{L} + \frac{V_i d}{L} \tag{3.24}$$

$$\frac{dVc}{dt} = \frac{iL}{C} - \frac{Vc}{RC} \tag{3.25}$$

Now the above equation can be written in state space representation as: The new variables will be introduced here. Let iL is replaced with x1, Vc is replaced with x2, d is replaced with u and y is replaced with Vc. Therefore, the state equation with the new variable can be rewritten as:

$$\frac{dx1}{dt} = \frac{-1}{L}x2 + \frac{Vi}{L}u \tag{3.26}$$

$$\frac{dx2}{dt} = \frac{1}{C}x1 - \frac{1}{RC}x2 \tag{3.27}$$

Here the input is Vi and the output is y=x2. By taking the Laplace transform of the above equation:

$$sX1 = \frac{-1}{L}x2 + \frac{Vi}{L}u \tag{3.28}$$

$$sY = \frac{1}{C}x1 - \frac{1}{RC}y \tag{3.29}$$

By rearranging the above equations, the transfer function of the buck converter is:

$$\frac{Y(s)}{Vi(s)} = D\left[\frac{\frac{1}{LC}}{S^2 + \frac{1}{RC}S + \frac{1}{LC}}\right] \tag{3.30}$$

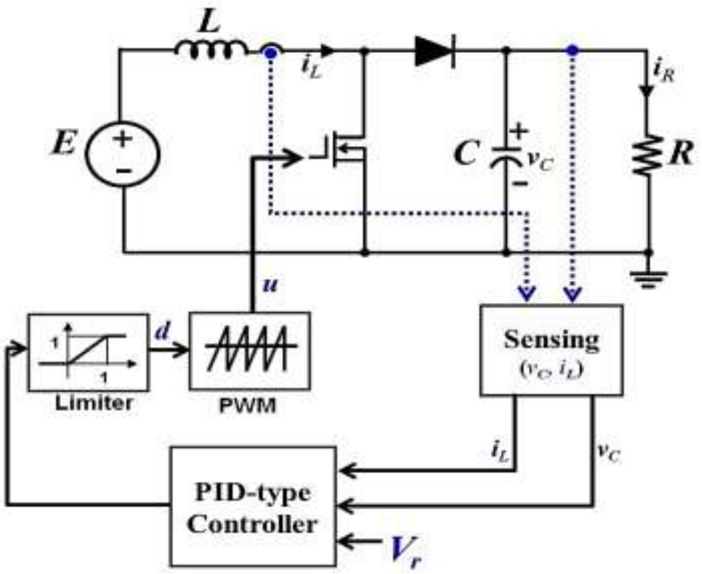

Figure 3.12 Load voltage (boost convertor) control by using PID controller

The above control uses the output voltage of the convertor as feedback and compares this output with the fixed reference value. Then, the error has given to the PID controller, which will then produce the corrected modulated voltage signal so that the buck convertor will produce a constant output voltage. The small signal single input single output transfer function used to control buck convertor ($G_c(s)$) given by:

$$G_c(s) = \frac{\frac{V_{in}}{LC}}{S^2 + \frac{S}{RC} + \frac{1}{LC}} \quad (3.31)$$

where, V_{in} is the input voltage for the buck convertor and R, L, and C are the resistance, inductance and capacitance for the buck convertor respectively.

In order to reduce the complexity and the noise effect of the D-controller, only the PI controller is considered for this research work. To determine the optimal gains of the PI controller fine tuning is applied (trial and error). And their values is shown in the following Table 3.7.

Table 3.7 PID control parameters for buck convertor.

Controller parameters	Tuned at (120V)
K_p	0.001
K_i	10

3.7.3. Maximum Power Point Tracker

The MPPT is used to improve the efficiency of the solar panel. The output power of any circuit can be maximized by adjusting source impedance equal to the load impedance according to maximum power point theorem. So, the algorithm of MPPT is equivalent to the problem of impedance matching. In this thesis, the Boost Converter is used as impedance matching device between input and output by changing the duty cycle of the converter circuit.

The output voltage of converter depends on the duty cycle. Therefore, MPPT is used to calculate the duty cycle for obtain the maximum output voltage because if output voltage increases than power also increases. In this thesis work Perturb and Observe (P&O) algorithm is used, because this requires less complexity and low-cost implementations.

3.7.3.1. Perturb and Observe MPPT Algorithm

Among other methods of MPPT, it is the simplest method to implement. It is easy to implement because in this method only voltage is sensed (Uma Shankar et al., 2013). Figure 3.13 shows flow chart of the perturb and observe MPPT. In this method, by varying the supplied voltage power output of system is checked. If an increasing the voltage, power also increases then further ‘δ’ is increased otherwise start decreasing the ‘δ'. Similarly, while reducing voltage if power increases the duty cycle is decreased. These steps continue till maximum power point is achieved. The corresponding voltage at which MPP is reached is called reference point (V_{ref}).

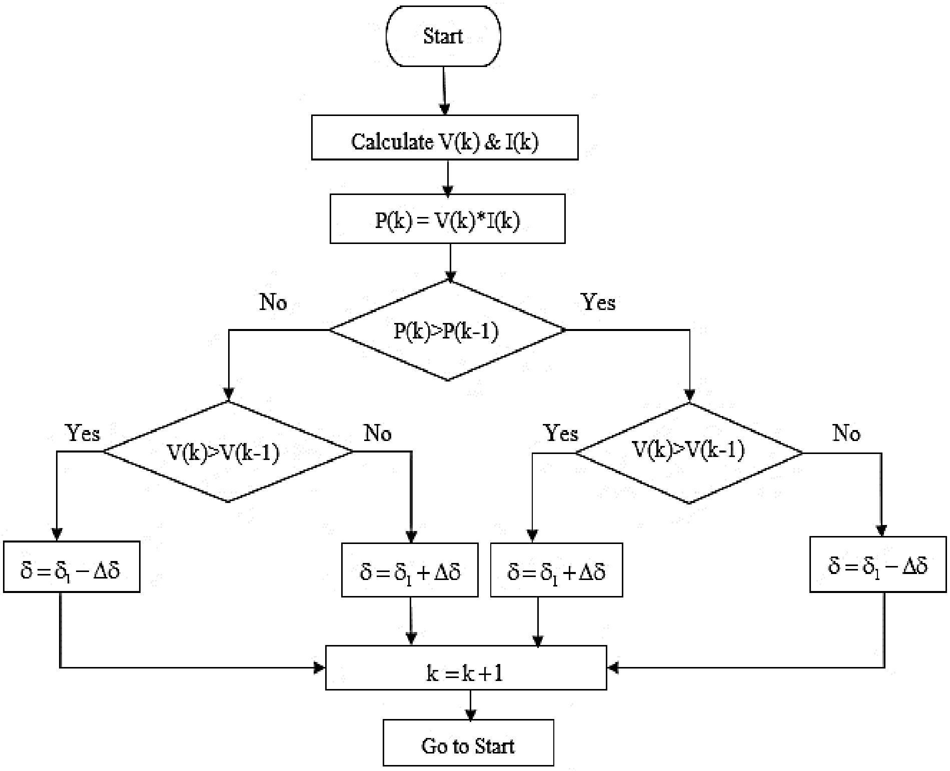

Figure 3.13 Flow chart of the perturb and observe MPPT (Uma Shankar et al., 2013)

3.7.4. Design of Energy Storage System

3.7.4.1. Lithium-ion Model

The storage capacity required for the battery bank depends on the number of days that the batteries can provide power to the load without recharging (Low Wen et al., 2014). Depth of Discharge (DOD) is the amount of energy drawn from a battery compared to its total storage capacity. For this system, DOD of 80% selected, which is typical for isolated PV storage systems. Its basic equivalent battery circuit equations are represented by shepherd's equation as (Emma Raszmann et al., 2017). The battery charging equation:

$$V_{batt}(t) = E_o - K\frac{Q}{Q - it}it - K\frac{Q}{it + 0.1Q}i^* + Ae^{-B\times it} \tag{3.32}$$

And its discharging equation:

$$V_{batt}(t) = E_o - K\frac{Q}{Q - it}it - K\frac{Q}{Q - it}i^* + Ae^{-B\times it} \tag{3.33}$$

The voltage at the battery terminal can be calculated as:

$$V_{batt} = E_{batt} - I_{batt} \times R_{batt} \tag{3.34}$$

Also, the exponential voltage (A) can be determined as,

$$A = V_{full} - V_{exp}$$

Exponential zonetime (B in 1/Ah) constant inverse can be related as;

$$B = \frac{2.3}{Q_{exp}}$$

$$K = 0.065 * \left[V_{full} - V_{nom} + A\left(e^{-B\times Qnom} - 1\right)\right] * \frac{Q_{full} - Q_{nom}}{Q_{nom}}$$

where: E_o - Battery voltage constant (V), Q - battery capacity (Ah), E_{batt} - Internal battery voltage (V), R - internal resistance (Ω), amplitude constant (V), its battery discharge capacity (Ah), and i^*-Filtered current through polarization resistance.

Battery state of charge can be expressed as;

$$SOC(t) = SOC(t-1) + \frac{i(t)\times \Delta t}{Q} \text{ (If Q is in Ah)} \tag{3.35}$$

The SOC can be expressed in other forms (Wh) as shown below;

$$SOC(t) = SOC(t-1) + \frac{P(t)\times \Delta t}{Q} \text{ (If Q is in } Wh\text{)} \tag{3.36}$$

Battery sizing: Battery capacity (in Ah) is determined by using the total load (in Ah) required per day and the number of days the system is required to operate without energy generation (Emma Raszmann et al., 2017). Number of days typically ranges from 2 to 6 (R.A.Dougal et al., 2002). If the load supplied is not critical, then one autonomy day is commonly used. In order to size the minimum capacity of battery bank, the estimated energy storage is first determined. Sizing of a battery bank needed to supply 80,340Wh per day for the DC load of the MSAG.

Step 1: Energy consumption of battery: (Emma Raszmann et al., 2017)

$$E_b = \frac{\text{Energy demand} \times \text{Days of autonomy}}{\text{efficiency} \times \text{DOD} \times \text{Nominal battery voltage}} \tag{3.37}$$

where: Energy demand (E_d) = 80340Wh/day, days of autonomy (N) = 2, ηbat = 85% = 0.85, depth of discharge = 0.65.

$$E_b = \frac{(80340 \text{ x } 2)}{0.85 \times 0.65} = 290{,}823.53\text{Wh/day}$$

Step 2: Battery Ampere hour capacity: Select the battery, which is any kind, 12V nominal and 200Ah rating from the specification of deep cycle battery.

$$C_{bat} = \frac{E_b}{V_{nominal}} = \frac{290{,}823.53}{120} = 2423.53\text{Ah}$$

Step 3: Battery required for parallel:

$$B_{parallel} = \frac{C_{bat}}{Ah_{\text{rating of battery}}} \tag{3.38}$$

$$B_{parallel} = \frac{2168.42}{200} = 12.12 \approx 13$$

Step 4: Battery required for Series (B_{series}) = $\frac{V_{system}}{V_{bnominal}} = \frac{120}{12} = 10$

Step 5: The total number of batteries required = $B_{series} \times B_{parallel} = 10 \times 13 = 130$

Therefore, the total batteries required is 130 batteries.

Table 3.8 Typical parameters of Hoppecke 4 OPzS 200 lithium-ion battery (Andreas Nyman et al., 2012)

Characteristics	Hoppecke 4 OPzS 200 battery
Specific energy (Wh/kg)	150 - 200
Ampere hour rating (Ah)	200
Nominal cell voltage (V)	12
Electrical efficiency (%)	85
Self-discharge (%)	0.1 - 0.3
Life time (years)	5

3.7.4.2. Charge Controller Sizing

The sizing of charge controllers is depending on the maximum charging current from the photovoltaic array and the current rating of the charge controller (Mohad Jadain et al., 2015) (T. M. Parimita, 2016).

$$\text{Current controller rating} = 1.25 \times I_{sc} \times N_p \quad (3.39)$$

$$\text{Number of charge controllers} = \frac{I_{controller\,rating}}{\text{Ampere of control from specification}} \quad (3.40)$$

where: 1.25 is the safety factor for sizing PV systems, I_{sc} is the short circuit current of the PV module, and N_p is the number of solar modules connected in parallel.

Therefore, the current controller rating = 1.25 × 8.68 × 51 = 553.35A. For this thesis work, 12V, 60Ah MPPT based solar charge controller were selected.

$$\text{Number of charge controllers} = \frac{\text{Total current controller rating}}{\text{Controller rating from specification}} \quad (3.41)$$

$$= \frac{553.35A}{60A} = 9.2225 \approx 10$$

3.7.5. Bidirectional DC-DC Converter Modeling

Bidirectional DC-DC converters are power electronics devices for the purpose of step-up or step-down the voltage level with the capability of flow power either in forward directions or in backward direction (Deepak Ravi al., 2018). They are useful for switching between energy storage and the DC bus. When the power demand is lower than the output of the solar panel, excessive energy will be stored in the battery, which is called charging mode.

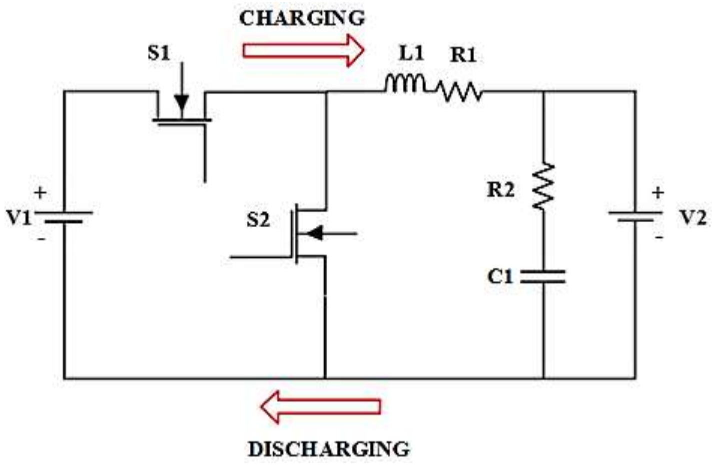

Figure 3.14 Circuit diagram of universal bi-directional buck-boost convertor

Conversely, when the power demand is higher than the output of the solar panel, energy flows from battery to the load, which is called discharging mode. This study proposes a bidirectional buck-boost converter to manage the storage and supply of power between photovoltaic power generation systems and batteries (Kuei Hsiang Chao et al., 2013). The charging/discharging mode defined as that the energy transferred from the DC bus to battery or from battery to DC-bus, since the battery voltage may be higher or lower than the DC-bus voltage during the entire operation. For buck converter the minimum inductance is calculated using Equation (3.42).

$$L = \frac{V_{bus} \times (V_{batt} - V_{bus})}{\Delta I_L \times f_s \times V_{batt}} \tag{3.42}$$

where, L is the inductor in the bidirectional DC-DC converter, V_{bus} is the bus voltage from the solar panel (66.3V), V_{batt} is the battery voltage or load voltage and its magnitude is 120V, and the switching frequency f_s is and its magnitude is considered to be 20,000Hz.

In order to determine the current ripple and the voltage ripple, the maximum current has to be determined first and its formula is shown in Equation (3.43).

$$I_o(\max) = \frac{P_{Load}}{V_{bus}} = \frac{4060W}{66.3V} = 61.24A \tag{3.43}$$

Hence usually the inductor current ripple has to be between 20 to maximum of 40% of the maximum load current. For this case the current ripple is considered as 30% of the maximum current.

$$\Delta I_L = (0.2 \text{ to } 0.4) \times I_o(\max) = 0.3 * 61.24A = 18.37A \tag{3.44}$$

Substitute each data in the Equation (3.42) and the inductor becomes;

$$L = \frac{66.3 \times (120 - 66.3)}{18.37 \times 20000 \times 120} = 80.75 \mu H$$

In order to be sure, the current stayed within the specified range, the capacitor should be determined carefully. The capacitor is calculated based on the Equation (3.45) shown below.

$$C_{batt}(\max) = \frac{\Delta I_L}{8 \times f_s \times V_{bus}(ESR)} \tag{3.45}$$

$$V_{bus}(ESR) = ESR \times \Delta I_L = 0.155\Omega \times 18.37A = 2.85V \tag{3.46}$$

Substitute Equation (3.46) in to Equation (3.45)

$$C_{batt}(\max) = \frac{18.37}{8 \times 20000 \times 2.85} = 40.28 \mu F$$

For boost converter the minimum inductance is calculated based on Equation (3.47) below.

$$L = \frac{V_{batt} \times (V_{bat} - V_{bus})}{\Delta I_L \times f_s \times V_{bus}} \tag{3.47}$$

Substitute each data in the Equation (3.47) and the inductor becomes;

$$L = \frac{120 \times (120 - 66.3)}{18.37 \times 20000 \times 66.3} = 0.2645\text{mH}$$

The bus minimum capacitor is calculated based on the Equation (3.48) shown below.

$$C_{bus}(\min) = \frac{I_o(\max) \times D}{f_s \times \Delta V_{bus}} \tag{3.48}$$

The duty cycle in case for the boost converter is determined as follows;

$$D = 1 - \frac{V_{bus}}{V_{batt}} = 1 - \frac{66.3}{120} = 0.4475$$

where, ΔI_L : estimated, inductor ripple current, a good estimation for inductor ripple is 20% to 40% of output current. $I_o(\max)$: maximum output current.

The maximum ripple bus voltage ΔV_{bus} is considered as 3% of bus voltage and its value is 3.978V. based on the above data the capacitor is determined as follows;

$$C_{bus}(\min) = \frac{61.24 * 0.4475}{20000 * 1.988} = 689.258\mu\text{F}$$

From the datasheet C_{batt} = 1000µF, C_{bus} = 1000µF, and L = 4mH is selected for the bidirectional buck boost convertor (Kou-Bin Liu et al., 2016).

Bi-directional Buck-Boost Controller: The main objective of the bidirectional converter controller is to control the energy storage system, to maintain a constant DC-bus voltage (Yen Yee Chia et al., 2015). The PID controller is used in order to determine a stable current and stable voltage at the load side and monitoring the battery state of charge (%SOC). From the PID controller output, the pulse width modulated signal is generated to toggle the power semiconductor switch based on the reference current and reference voltage.

3.7.6. DC Link Design

This method of calculating a minimal capacity of the DC link capacitor depends on the expected maximum input power step and the definition of a limit of allowed voltage deviation. A widely-used limit is a deviation of ten percent of the DC link voltage at any step-on and step-off load response. The expected maximum input power step is equal to the solar panel power at the maximum power point (MPP). The time constant T_r stands for the control delay of the DC/DC converter and for instance a value of about five to ten modulation periods is a good choice (H. Raffel, 2017). This method starts with the energy ΔW which is estimated as:

$$\Delta W = \int_0^{T_r} \Delta P_{max} . dt = \Delta P_{max} . T_r \tag{3.49}$$

The stored energy of the capacitor can be written as follows:

$$W = \frac{1}{2} C_d V_d{}^2 \tag{3.50}$$

The variation of the stored energy in the capacitor also depends on the DC link voltage V_d, the DC link voltage deviation ΔV_d and the capacity C_d and can estimated:

$$\Delta W = \frac{1}{2} C_d (V_d + \Delta V_d)^2 - \frac{1}{2} C_d V_d{}^2 \tag{3.51}$$

The combination of the Equations (3.49) and (3.51) leads to the expression of the minimal capacity $C_{d,min}$:

$$C_{d,min} \geq \frac{T_r . \Delta P_{max}}{(V_d \Delta V_d + \frac{1}{2} \Delta V_d{}^2)} \tag{3.52}$$

Another method to appreciate the minimal DC link capacity is given in (H. Raffel, 2017), where the exchanged energy ΔW by the capacitor bank is estimated as follows:

$$\Delta W = \frac{T_r . \Delta P_{max}}{2} \tag{3.53}$$

The voltage deviation is given by:

$$\Delta V_d = \frac{\Delta W}{C_d V_d} \tag{3.54}$$

Finally this leads to another equation of the minimal capacity $C_{d,min}$:

$$C_{d,min} \geq \frac{T_r . \Delta P_{max}}{2 . V_d \Delta V_d} \tag{3.55}$$

Comparing the Equations (3.52) and (3.55) and assuming a DC link voltage deviation ΔV_d of commonly used ten percent, it can be seen that, the appreciation of delivers nearly twice the values of the minimum capacity (H. Raffel, 2017).

3.7.7. Cable Sizing

Cable sizes are particularly necessary for low voltage batteries, solar panels cables, and load cables.

Table 3.9 Values of parameters used for cable sizing

Description	Value
Length of cable	4m
Conductivity of copper	58×10^{-6} s/m
Resistivity of copper	$1.72 \times 10^{-8}\ \Omega$

It must be properly sizing otherwise if it is far too small, so it can be dangerous and leads to heat up and potentially cause a fire and waste energy. The following steps are followed to determine the cable size (T. M. Parimita Mohant et al., 2016). Cables must cause less than 3% voltage loss between PV modules and battery charge regulator calculated as:

3.7.7.1.Cable Size Between Solar PV Array and Battery

The maximum controller DC is defined as 125% times the rated short-circuit current (I_{sc}) from PV specification.

$$I_{max} = 1.25 \times 8.68 \times 22 = 238.7\text{A}$$

Generally, the cross-sectional area of the cable is given by the following Equation [59].

$$A = \frac{2 \times L \times I_{max}}{\text{Conductivity} \times V_{drop}} \tag{3.56}$$

where: ρ is the resistivity of copper wire, V_d is the maximum allowable voltage drop, L is the length of the cable and, I_{max} is the maximum current that can be carried by the cable or the conductor.

$$A = \frac{2 \times 4 \times 238.7}{58 \text{x} 10^{-6} \frac{s}{m} \text{ x } 0.03 \times 120} = 9.15\text{mm}^2$$, Therefore, 10mm^2 is chosen from cable standard.

3.7.7.2. The Cable Size Between Battery to Load

Considering the length of the cable as 2m between battery to load and the allowable voltage drop is 4 %. In such cases, the cross-sectional area is determined by using the following equation as follows (Mohad Shawal Jadin et al., 2015). The maximum current from battery at full load supply is given by:

The maximum charge controller to load current = $\frac{\text{Total load power}}{\text{Load voltage}} = \frac{4060\text{W}}{48\text{V}} = 84.6\text{A}.$

To calculate the cable size between load and charge controller, the given voltage losses are 5% of 48v, length 2m, and 84.6A. using Equation (3.57) the area of the cable is (Mohad Shawal Jadin et al., 2015) (T. M. Parimita Mohant et al., 2016):

$$A = \frac{2 \times L \times I_{max,load}}{Conductivity \times V_{drop}} \tag{3.57}$$

where, $I_{max,\ load}$ is the maximum load current.

$A = \frac{2 \times 2 \times 84.6}{58 \times 10^{-6} \times 0.05 \times 48}$ = 2.43mm^2, thus the chosen area is 2.5mm^2 from cable standard.

The following Table 3. 10 shows the analysis summary of PV system component sizing.

Table 3.10 A summary for PV system component sizing

Component	Description of component	Result
Load	Total estimated load (kW)	4.08
	Total estimated energy (kWh)	80.34
PV Array	Capacity of PV array (kW)	20.91142
Number of modules in series		3
Number of modules in parallel		51
Total number of modules		153
Battery bank	Battery bank capacity (Ah)	2168.42Ah
Number of batteries in series		11
Number of batteries in parallel		10
Total number of batteries required		121
Number of charge controllers		10
Wire (mm^2)	Between PV modules and batteries	10
	Between batteries and load	2.5

3.8. Economic Analysis

In this section the life cycle cost (LCC) estimation of the designed stand-alone PV system is discussed. The initial capital cost of the system is the cost that is required for purchasing all system components, such as PV panel, battery, charge controller, converter, and installation (including wiring and others). Operation and maintenance (O and M) costs are also annual periodic expenses for system management, site supervision, and regular maintenance (M. Boxwell, 2017). The following assumptions are considered for calculating the stand-alone PV system cost.

- The capital cost of the system (initial cost) is high,
- Maintenance costs are very low,
- There are no fuel costs, and
- Replacement costs are low (especially for batteries).

The life time N of all the items is considered to be 25 years, except that the battery which is considered to be 5 years. Thus, an extra 2 group batteries (each of 2 batteries) have to be purchased, after 5 years, 10 years, 15 years, and 20 years. Assuming an inflation rate i is 4% or 0.04 and discount rate (d) of 10%. Therefore, the present worth (PWs) of all the items can be calculated as follows (M. Boxwell, 2017):

- PV panel initial cost (C_{PV}) = 2\$/W × 153 × 140W = \$42,840
- Initial cost of batteries (C_B) = \$0.24/Ah x 200Ah x 121 = \$6,336
- The PW of the first extra group of batteries (purchased after N = 5 years), C_{B1PW} can be calculate as (M. Boxwell, 2017):

$$C_{B1PW} = C_B \left(\frac{1+i}{1+d} \right)^N \tag{3.58}$$

$$C_{B1PW} = \$6336 \left(\frac{1+0.03}{1+0.1} \right)^5 = \$4560.77$$

- The PW of the 2nd extra group of batteries (purchased after N = 10years) $C_{B2PW,}$ the 3rd extra group of batteries (purchased after N = 15years) $C_{B3PW,}$ and that of the 4th extra group of batteries (purchased after N = 20years) C_{B4PW} are calculated, using Equation (3.58), to be \$3282.92, \$2363.11, and \$1701.01 respectively.
- Cost of converter (C_C) = \$1567.42
- Cost of charge controller (C_{CC}) = \$16.996 x 10 = \$169.96
- Installation cost C_{Inst} = 0.1 x \$42,840 = \$4,284.
- The PW of the maintenance cost C_{MPW} can be calculated using the maintenance cost per year (M/yr) and the life time of the system (N = 25 years). And maintenance cost is taken to be 2% of the total PV cost, which is equal to \$856.8.

$$C_{MPW} = \left(\frac{M}{yr}\right) \times \left(\frac{1+\mathrm{i}}{1+\mathrm{d}}\right) \times \left(\frac{1-\left(\frac{1+\mathrm{i}}{1+\mathrm{d}}\right)^{N}}{1-\left(\frac{1+\mathrm{i}}{1+\mathrm{d}}\right)}\right) \quad (3.59)$$

$$C_{MPW} = \$856.8 \times \left(\frac{1+0.03}{1+0.1}\right) \times \left(\frac{1-\left(\frac{1+0.03}{1+0.1}\right)^{25}}{1-\left(\frac{1+0.03}{1+0.1}\right)}\right) = \$10,170.89$$

Therefore, the LCC of the system can be calculated as the following Equation (3.60).

$$LCC = C_{PV} + C_{B} + C_{B1PW} + C_{B2PW} + C_{B3PW} + C_{B4PW} + C_{C} + C_{Ins} + C_{MPW} + C_{S} \quad (3.60)$$

$$LCC = \$42,840 + \$6,336 + \$3,282.92 + \$2,363.11 + \$1,701.01 + \$1,567.42 + \$169.96 + \$4,284 + \$10,170.89 + \$23,198.21$$

$$LCC = \$95,913.52$$

It is always useful to calculate the LCC of a system on annual basis. The annualized LCC (ALCC) of the PV system in terms of the present-day dollars can be calculated using the following Equation (3.61) (M. Boxwell, 2017).

$$ALCC = LCC\left(\frac{1-\left(\frac{1+\mathrm{i}}{1+\mathrm{d}}\right)}{1-\left(\frac{1+\mathrm{i}}{1+\mathrm{d}}\right)^{N}}\right) \quad (3.61)$$

$$ALCC = \$95,913.52\left(\frac{1-\left(\frac{1+0.03}{1+0.1}\right)}{1-\left(\frac{1+0.03}{1+0.1}\right)^{25}}\right) = \$7,565.62$$

Once the ALCC is known, the unit electrical cost (cost of 1 kWh) can be calculated, to be \$0.238/kWh, from Equation (3.62):

$$Unit\ Electrical\ Cost = \frac{ALLC}{365E_L} \tag{3.62}$$

$$Unit\ Electrical\ Cost = \frac{\$7565.62}{365 \times 80.34kWh/yr} = \$0.258/kWh$$

It is to be noted that, this price is high as compared to the current unit cost of electricity in Ethiopia. PV energy generation for the MSAG is very crucial and important due to its better efficiency and reliability to the power distribution for the MSAG. This price is also free from interruption and fuel cost.

3.8.1. HOMER Software PV System Design

The following figure shows the integration of the three power supplies and the air conditioner or fan of the MSAG system in HOMER software. The system design includes convertor, battery, PV system, and the loads as shown in Figure 3.15.

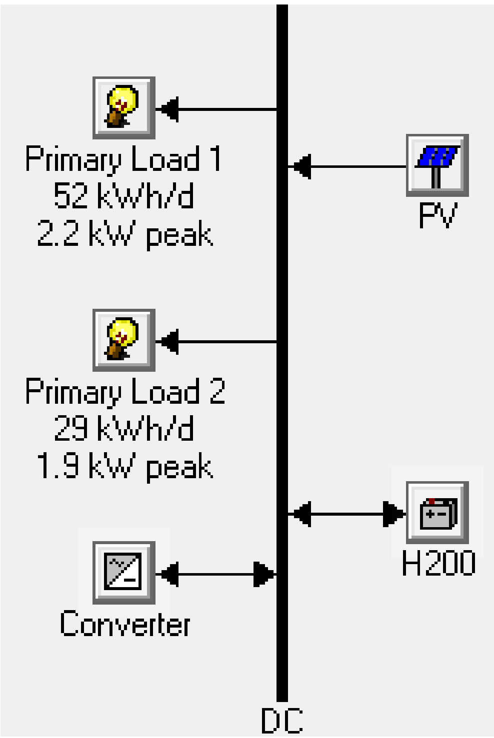

Figure 3.15 Interconnected PV power system in HOMER

The solar irradiation of the Adama City is applied to the solar assessment in HOMER and the monthly versus daily radiation graph is shown in the following Figure 3.16.

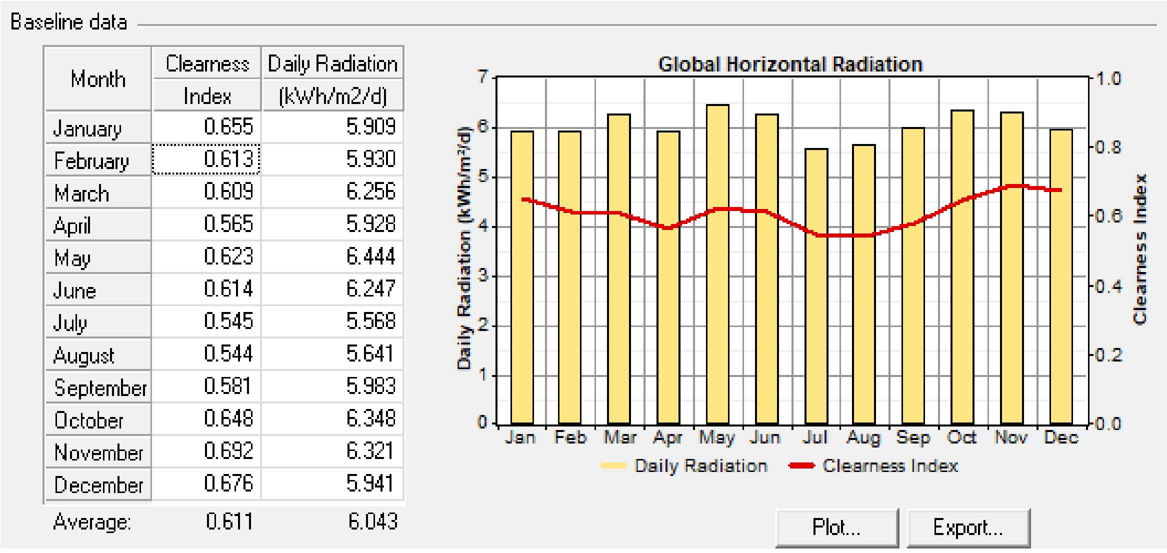

Figure 3.16 Solar irradiation data and its data graph in HOMER

The primary loads (load 1 and 2) setup is implemented in the HOMER as shown in the following Figures 3. 17 and 3.18. The random variability parameters which are day to day and time step to time step are considered to 0.001% in both cases.

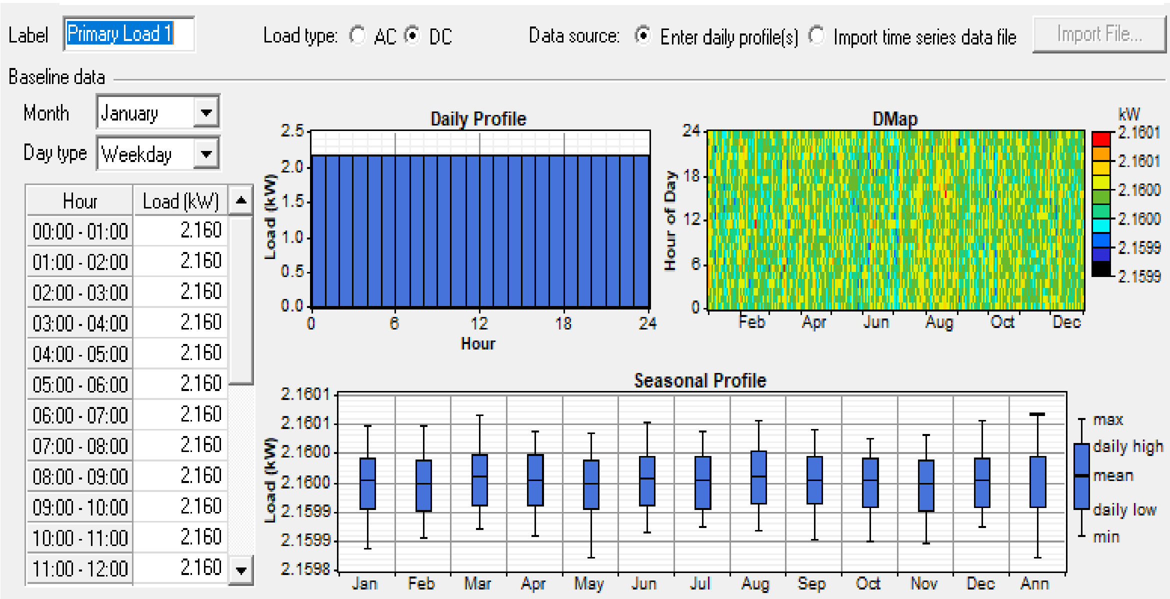

Figure 3.17 The primary load 1 setup configuration

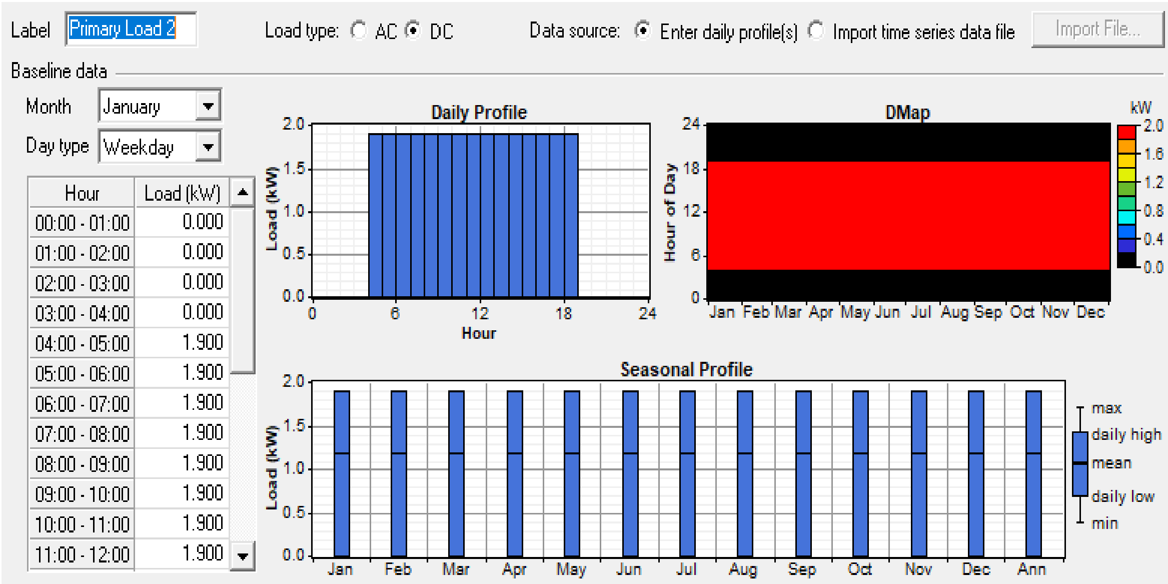

Figure 3.18 The primary load 2 setup configuration

A Hoppecke 4OPzS 200 battery type is chosen and its setup is shown in the following Figure 3.19. According to the current price which is 12v and 200Ah capacity is $48. So, in order to find the optimal cost, the analysis is done based on the different battery numbers which are below and above the required number of batteries (121). The battery per string for this specific battery type is considered as 6 each of having 2v capacity with the minimum of 5years life.

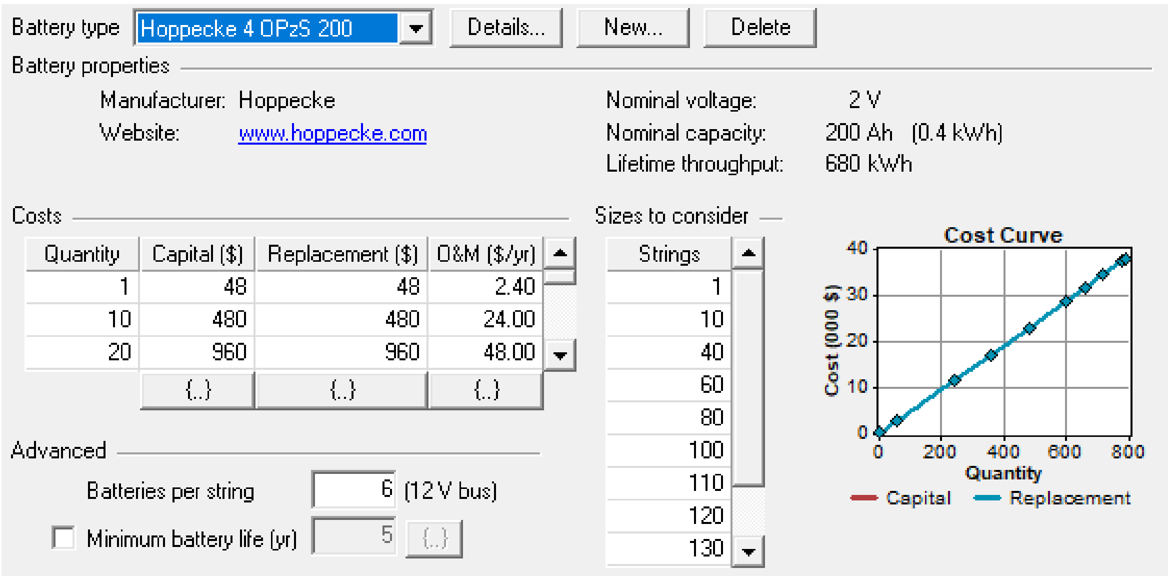

Figure 3.19 Hoppecke 4 OPzS 200 battery type configuration in HOMER software

3.9. Selection of Protective Devices

Besides the major component selection, safety measures are equally important for the solar PV system for which the protective devices to be used need to be selected properly. Failure to do so may not only lead to system efficiency but also may pose severe safety hazards. Typical protection devices which are to be selected carefully are as follows:

3.9.1. PV Source Circuit Combine Box and PV Fuse Disconnect

These fuses or circuit breakers are installed to protect the PV modules and wiring from excessive reverse current flow that can damage PV cell interconnects and the wiring between the individual PV modules. The rating of the fuse is specified by the PV module manufacturer. As per the NEC requirement for over current protection, the fuse rating marked on the back of the PV module must be at least 156 % of short-circuit current (I_{sc}) of the PV module at STC. The fuse will generally be a dc-rated cartridge-type fuse that is installed in a finger-safe pull out-type fuse holder.

3.9.2. Grounding

Grounding is one of the most critical tasks in the entire installation of a solar PV system. Grounding means connecting a part of the system's structure and/or wiring electrically to the earth. Grounding of a system does four things:

- It discharges accumulated charges.
- If lightning does strike, the ground connection provides a safe path for discharge directly to the earth rather than through the wiring.
- It reduces shock hazard from the higher voltage parts of the system, and
- It reduces electrical hum and radio caused by converters, motors, fluorescent lights and other devices.

3.9.3. Lighting Arrestor

In locations susceptible to lightning strikes, a lightning protection system must be provided, and all the exposed metallic structures of the solar PV system must be bound to the earthing system, and structures and PV module frames must be properly grounded. In certain geographical locations, solar PV systems might be exposed to the threat of lightning strikes. As lightning can cause damage to the PV modules and converters, extra care must be required to ensure that proper lightning protection is provided for the solar PV system and the entire structure. The inverters should be protected by appropriately rated surge arrestors on the DC system.

3.9.4. Surge Protector

Surge protection devices bypass the high voltages induced by lightning. They are recommended for additional protection in lightning-prone areas or where good grounding is not feasible (such as on a dry rocky mountain top), especially if long lines are being run to an array, pump, antenna, or between buildings. To reduce the possibility of a fire and to protect the system from a damage caused by lightings, it is recommended to have a voltage-clamping device across the DC bus bar. A metal oxide varistor (MOV) is commonly used in such applications.

CHAPTER FOUR

RESULTS AND DISCUSSIONS

In this section the result obtained is discussed briefly. In the MATLAB Simulink model, the selected PV module is Kyocera Solar KD140GX-LFBS. Each module has a capacity of 140Wp. The total number of modules required is 153 modules and from which 3 are conned in series and 51 are connected in parallel. The PV array used in this research work is a 4.06kW power.

4.1. PV Array Output Results

At the standard condition irradiation and temperature 3x51 modules are connected to generate the required power of the system. For the solar PV of 4.06kW is the combination of the 140W with 3 modules in series and 51 modules in parallels. The output curve of current versus voltage of the system module of Kyocera Solar KD140GX-LFBS 140W at standard condition is shown in Figure 4.1 below.

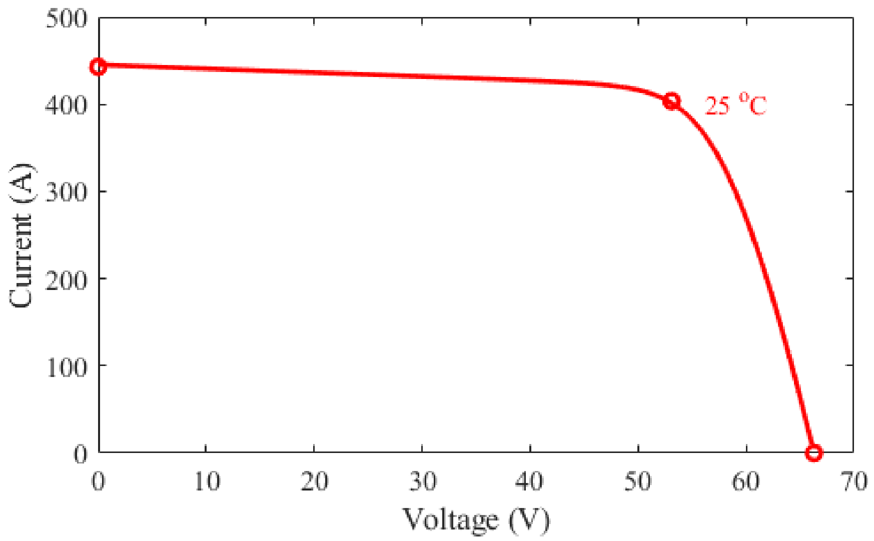

Figure 4.1 Current versus voltage characteristic curve of the module

Also, power versus voltage characteristic curve of the system module at standard condition is shown in Figure 4.2. The value of resistance connected in series with the solar cell as 0.23219Ω and the value of the shunt resistance connected in parallel to the cells selected as 37.4044Ω. The constant 1,000 W/m^2 and 25^{0}C given as input is the irradiation and temperature respectively. The system is simulated with various range of resistors connected to it, in this condition.

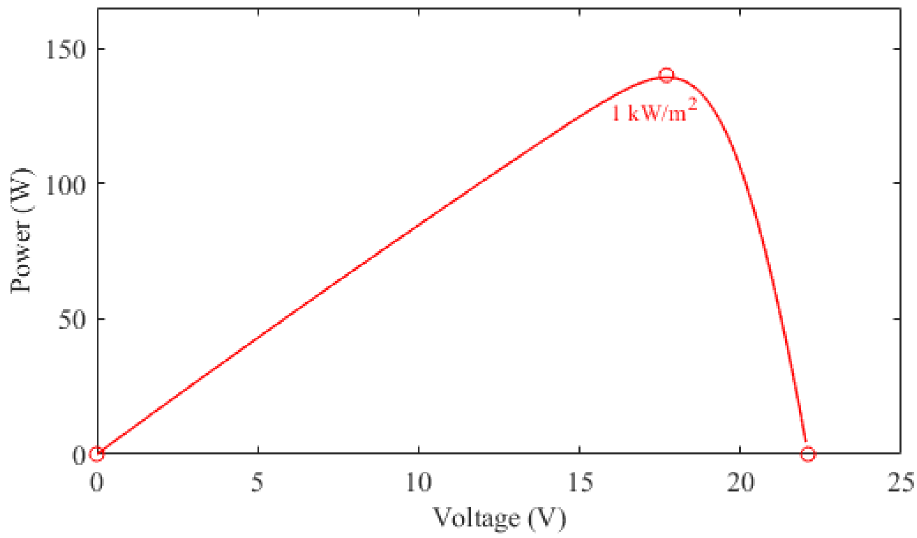

Figure 4.2 Power versus voltage characteristic curve of the module

The operating temperature affects the performance of the PV module. By varying the operating temperature and making irradiation constant the effect of temperature is observed. The values of operating temperature are set at 25^0C, 50^0C, 75^0C, and 100^0C at constant irradiation of $1000W/m^2$. The I-V and P-V characteristics of PV array at different temperature and constant irradiation is shown in Figure 4.3 and Figure 4.4 respectively.

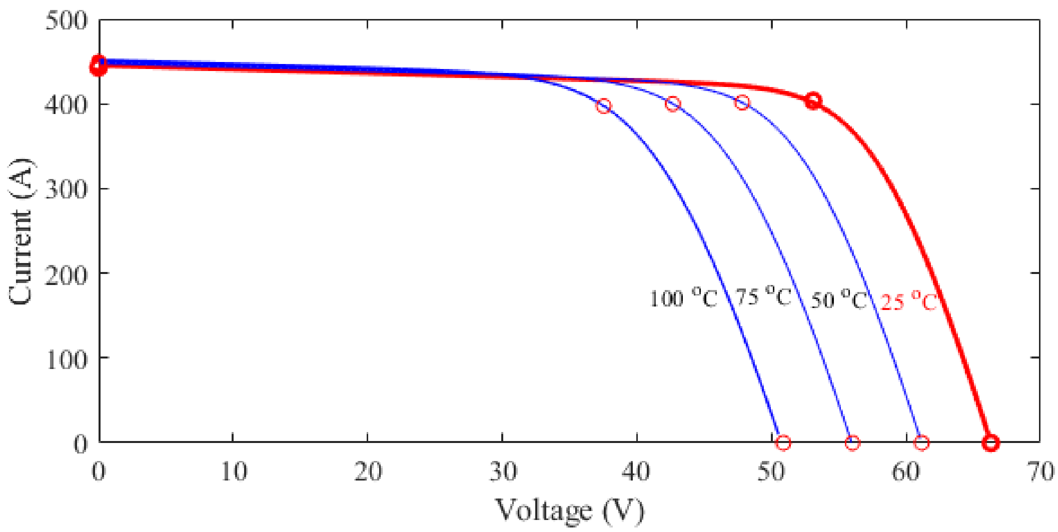

Figure 4.3 I-V characteristic of PV array at different temperature

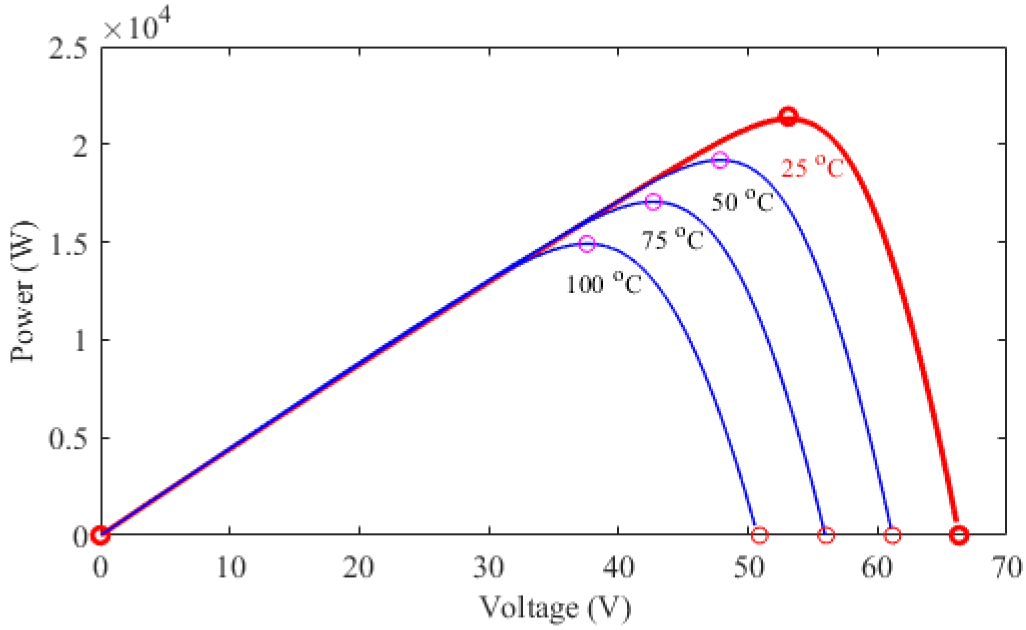

Figure 4.4 P-V characteristic of PV array at different temperature

The influences of temperature on the PV characteristics are observed in Figure 4.3 and Figure 4.4 above. As seen from the influence of the operating temperature on the open circuit voltage, there is the main effect of increase in cell temperature which decreases linearly with the cell temperature. Thus, the cell efficiency drops. As can be seen, with the increase of the cell temperature, the short circuit current increases slightly.

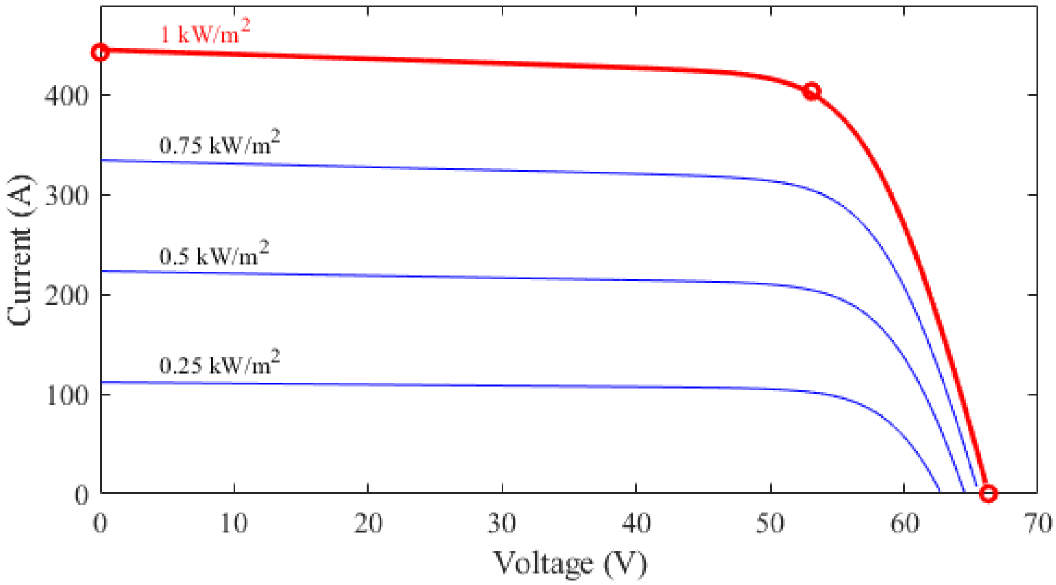

Figure 4.5 I-V characteristic of PV array at different irradiance

The solar irradiation also affects the performance of the PV module. By varying the solar irradiation and making temperature constant the effect of solar irradiation can be observed. The values of operating irradiance are set at 250W/m^2, 500W/m^2, 750W/m^2 and 1000W/m^2 at constant operating temperature of 25^{0}C. The I-V and P-V characteristics of PV array at different solar irradiation and constant operating temperature is shown in Figure 4.5 and Figure 4.6.

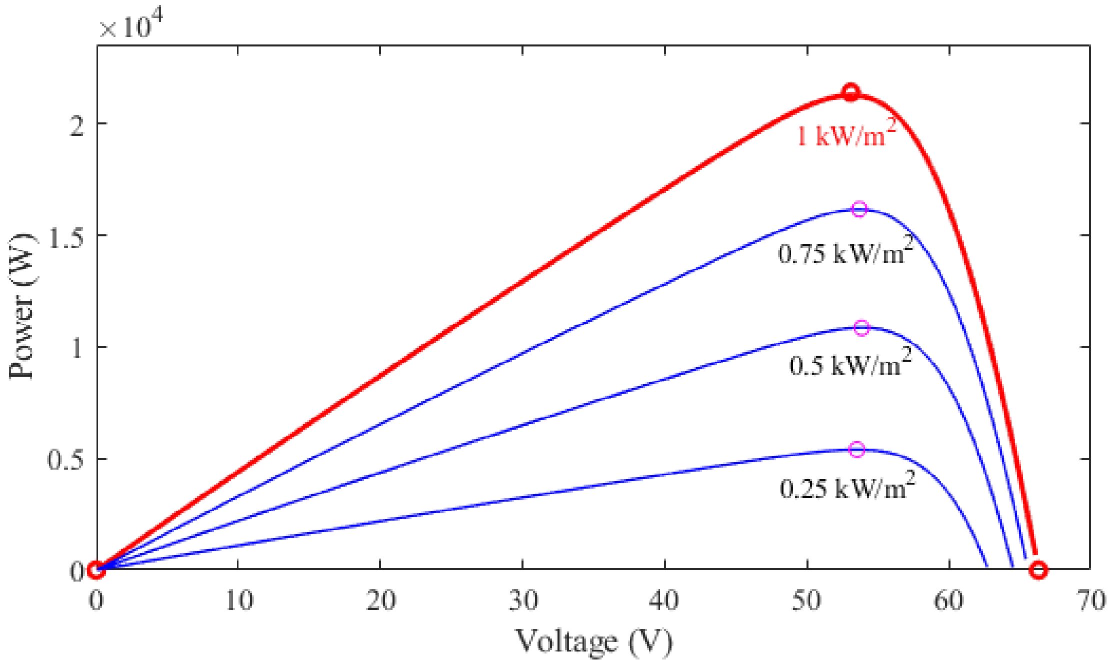

Figure 4.6 P-V characteristic of PV array at different irradiance

From the above Figure 4.5 and Figure 4.6 the influences of solar irradiation on PV module is observed. As seen from the above figure, by increasing the solar radiation, open circuit voltage increases logarithmically whereas the short circuit current increases linearly.

4.2. MATLAB/Simulink Simulation Results

In this thesis work, the system is simulated at the different atmospheric conditions with various solar irradiation. During the system simulation, there was some fluctuation of power, because of this, the proposed P&O algorithm provided a faster response by tracking the MPP under variable irradiance. The PV output voltage, and boosted output (load voltage) voltage of the stand-alone PV system is shown in Figure 4.7. And these parameters were controlled by using the MPPT P&O algorithm. As explained in the previous chapter the output voltage of the solar panel is approximately 66V, and the output of the boost converter is 120V. As it is shown that the PV array voltage has a direct relationship to solar irradiance. However, the solar irradiance is very low during the night and early morning. Therefore, the PV array voltage is almost reduced to zero.

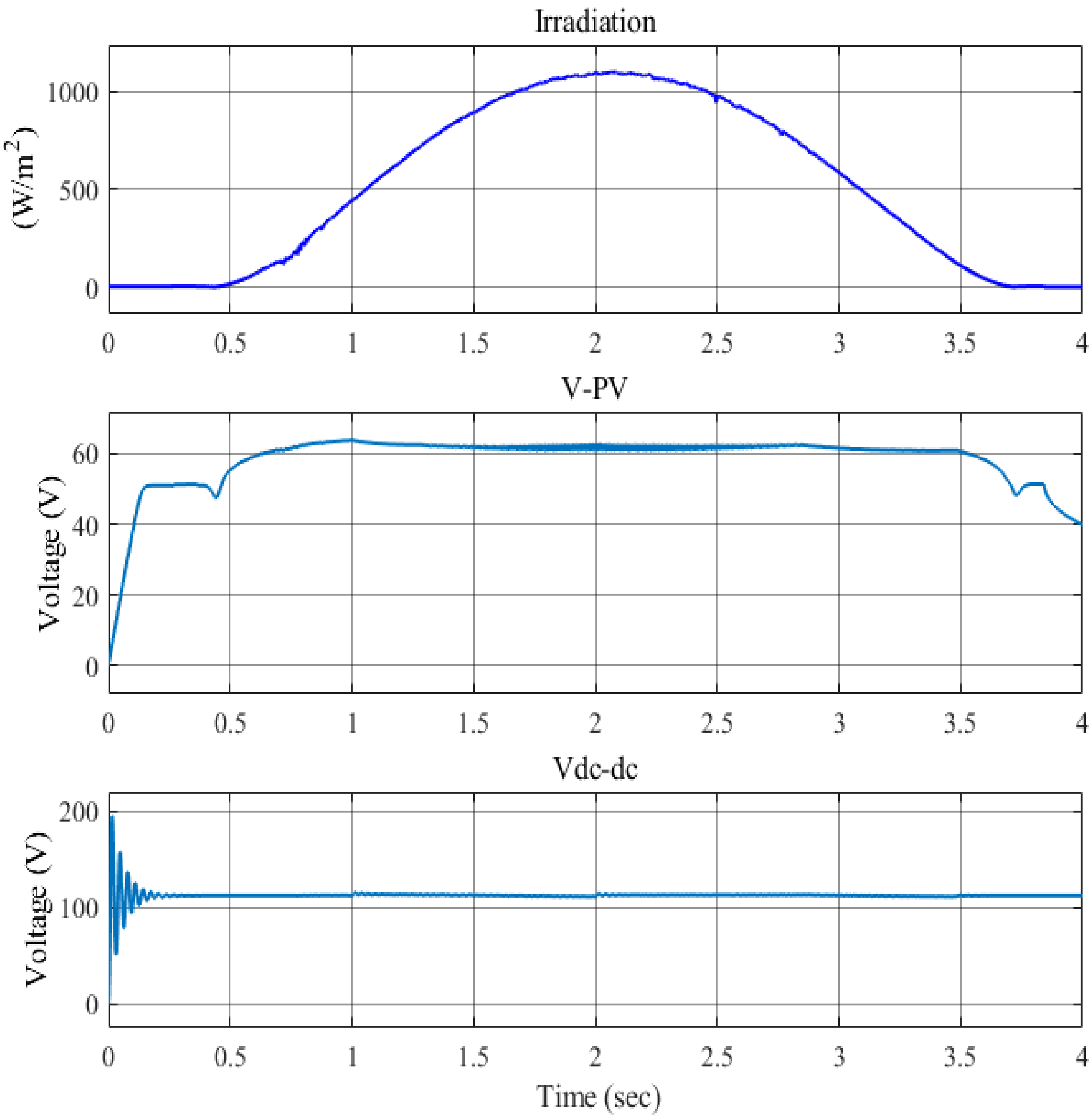

Figure 4.7 PV and boost DC-DC output voltages

The following results in Figure 4.8 are the load voltage, load curnet and load power. As can be seen when the irradiance is variable the current and the load power is variying at the same time. based on the load voltage and the load current, the load power is extracted. At the recommended level of irradiance the load curnet tries to increase and the load power as well. Hence from the given information the average load power is about 4.1kW which is approximately eqaul to the required load shown in Table 3.4.

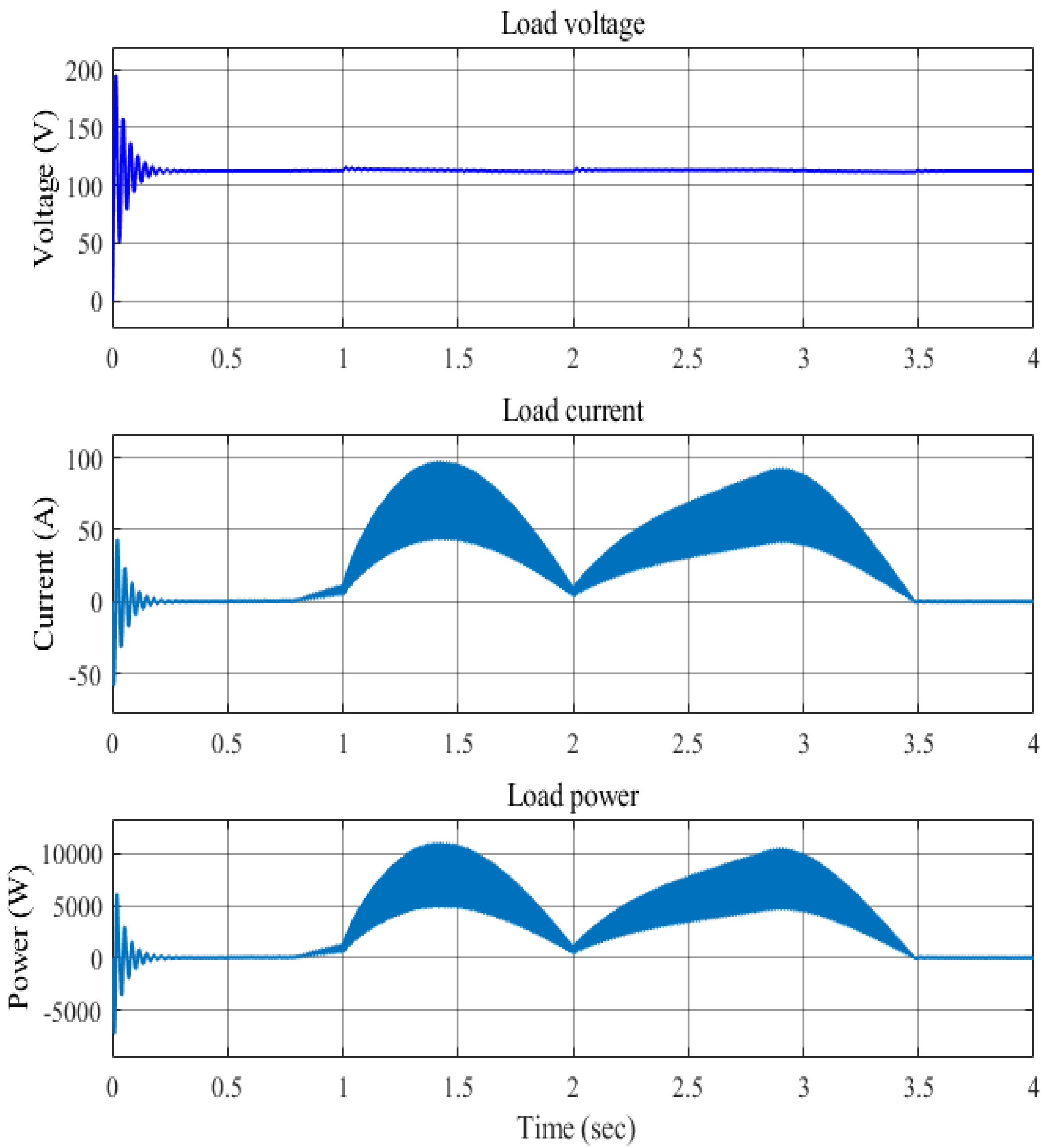

Figure 4.8 Load volage, load current, and load power

The battery voltage and current are also dependent on the irradiance level. At the start of the simulation the irradiance is very low and the output voltage is less than the battery voltage. At this point the battery is supplied the load and starts to discharge. When the battery is in discharging mode voltage starts to decrease as shown in Figure 4.9. When the solar panel has gotten enough irradiance, the battery starts charging and at this point the load voltage is greater than the battery voltage. And its voltage is starts to increase and the %SOC as well.

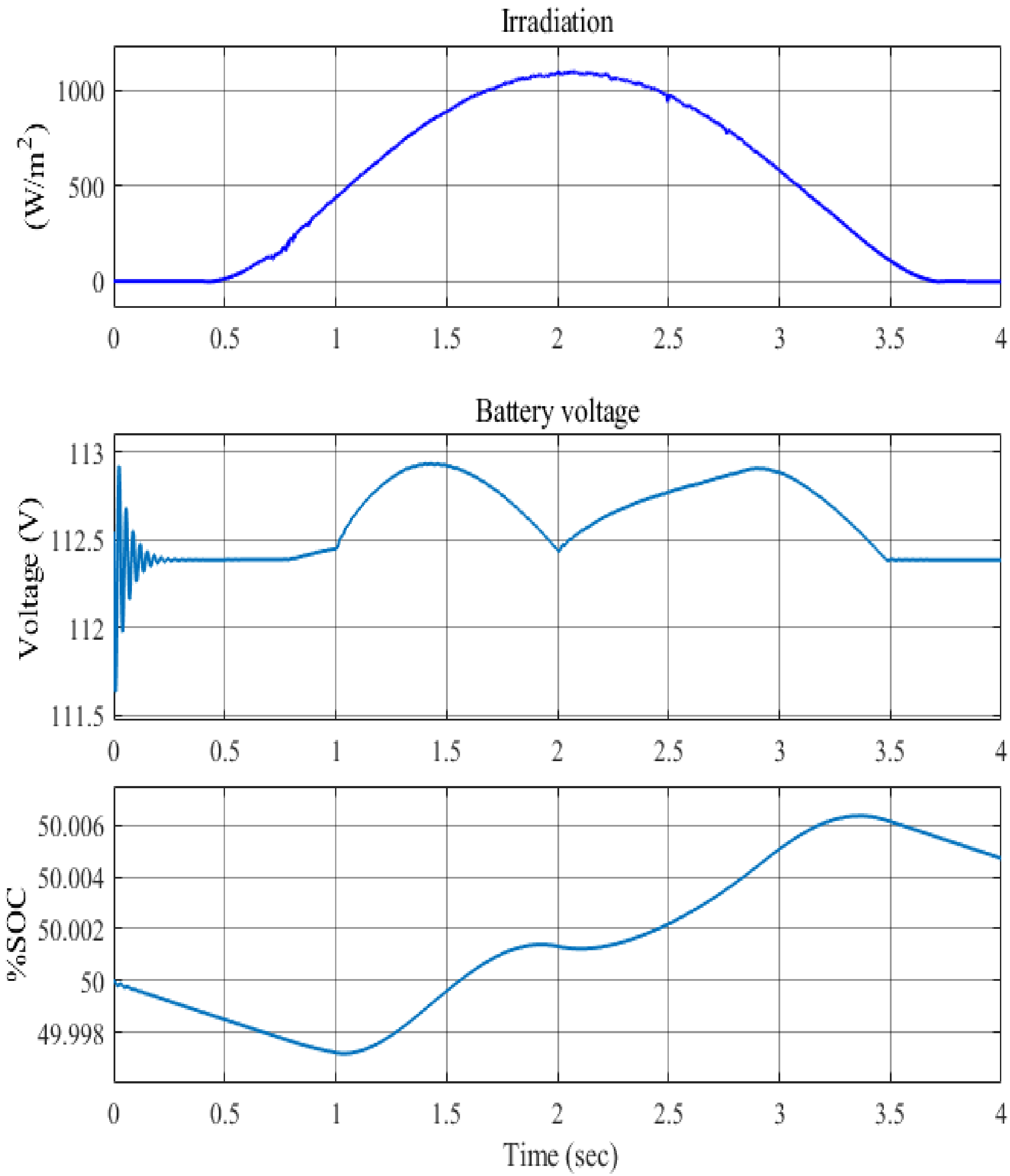

Figure 4.9 Battery voltage and state of charge

Also, the result of the battery current and the battery power vurses laod power results with %SOC are shown in the following Figure 4.10. When the battery is in charging mode the cueernt battery current is decreasing and going to be negative, meaning the battery is now becoming energy consumer. At this point the load power is increased because the irradiance is increased and the load voltage as well. However, the battery power is increased in the negative direction which shows the battery is in charging mode. When the battery is in discharging mode the battery power is positive and the battery current starts to increase in the positive direction.

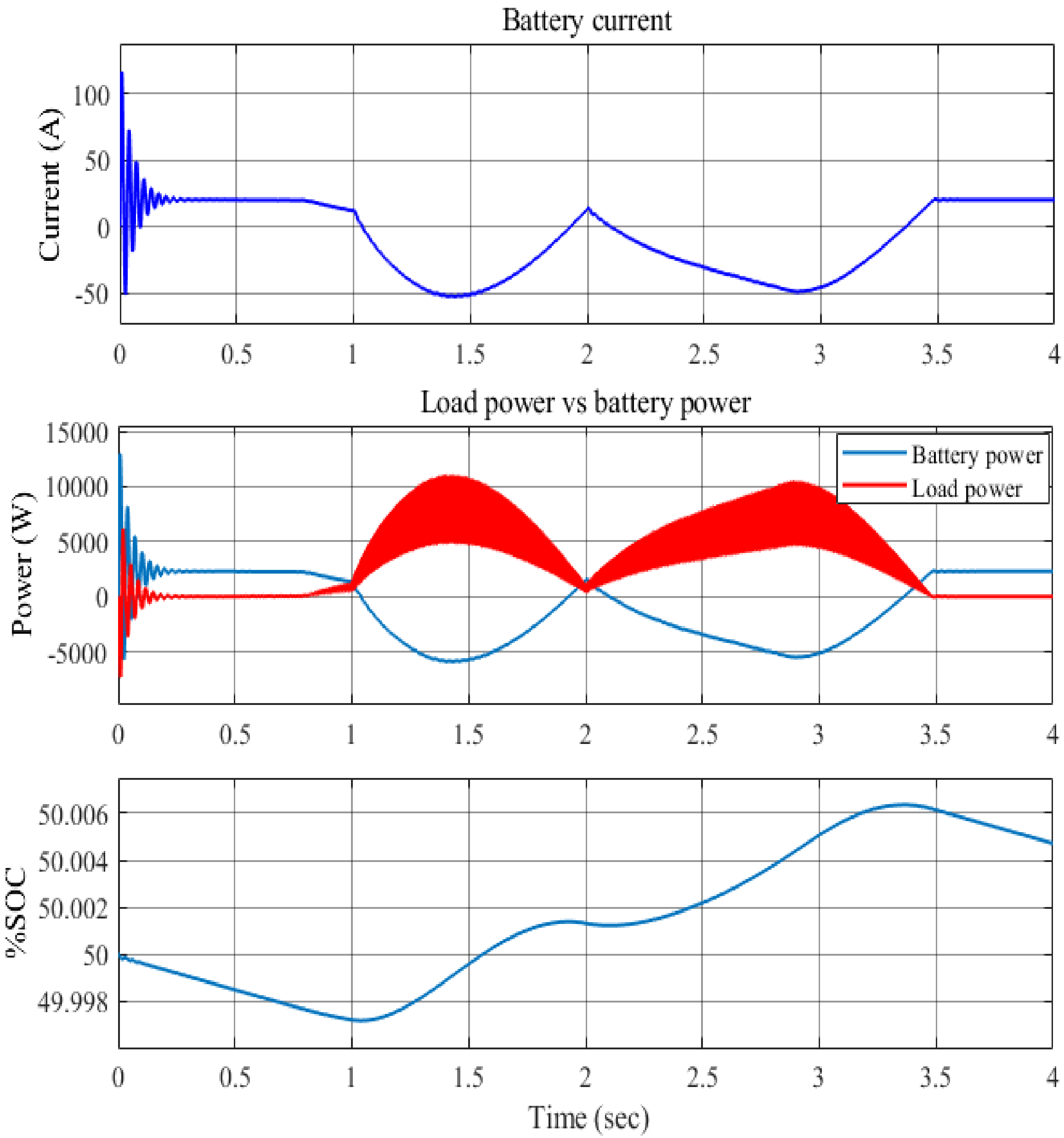

Figure 4.10 Battery current, load vs battery power and %SOC.

The battery characterisitc has been analysied and its system model is made of Lithium-ion Iron Phosphate (LFP) cells of 12V, 200Ah. They are arranged in several modules of cells connected in series to form a battery string of 120V. The battery system of the model has 11 battery strings in parallel to form a system rated energy at 80.34kWh. The battery system discharge characteristics are shown in Figure 4.11

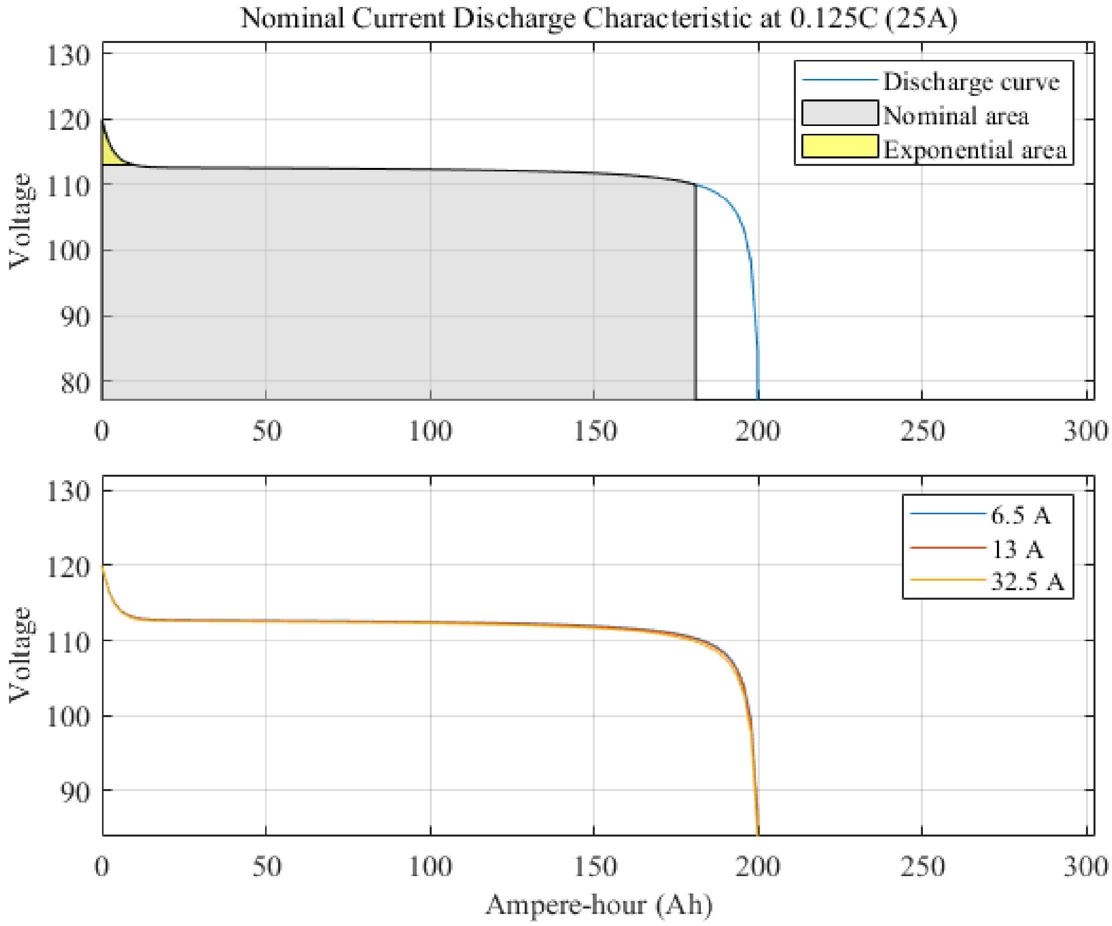

Figure 4.11 Battery system discharge characteristics

4.3. HOMER/Beta Simulation Result

The output of the HOMER simulation contains different combinations for each component and offers a list of feasible schemes depends on the values of the net present cost and cost of energy. The optimization result for this research work has two main groups which are sensitivity (different condition) results and overall cost analysis results.

4.3.1 Overall Cost Analysis

The overall optimization results for Multi-service Access Getway (MSAG) at Adama city were shown in Figure 4.12 below. As seen from the following figure the total cost per kWh is $0.258 under different circumstances. The HOMER software takes different sensitivity conditions and step time changes, as a result the calculated and the simulation result has a similar cost value.

PV (kW)	H200	Conv. (kW)	Initial Capital	Operating Cost ($/yr)	Total NPC	COE ($/kWh)	Ren. Frac.	Capacity Shortage
35.00	360	5.1	$ 95,880	2,756	$ 156,567	0.243	1.00	0.00
20.00	780	5.0	$ 84,440	3,283	$ 156,733	0.243	1.00	0.00
20.00	780	5.1	$ 84,540	3,286	$ 156,915	0.243	1.00	0.00
29.00	600	2.0	$ 91,700	3,007	$ 157,914	0.245	1.00	0.00
20.00	792	5.0	$ 85,016	3,318	$ 158,078	0.245	1.00	0.00
25.00	660	5.0	$ 89,180	3,133	$ 158,183	0.245	1.00	0.00
20.00	792	5.1	$ 85,116	3,321	$ 158,260	0.245	1.00	0.00
25.00	660	5.1	$ 89,280	3,137	$ 158,365	0.245	1.00	0.00
40.00	240	2.0	$ 97,520	2,772	$ 158,576	0.246	1.00	0.00
25.00	720	2.0	$ 89,060	3,196	$ 159,445	0.247	1.00	0.00
30.00	600	2.0	$ 93,800	3,047	$ 160,895	0.249	1.00	0.00
29.00	600	4.0	$ 93,700	3,081	$ 161,557	0.250	1.00	0.00
40.00	240	4.0	$ 99,520	2,847	$ 162,220	0.252	1.00	0.00
35.00	480	2.0	$ 98,540	2,897	$ 162,345	0.252	1.00	0.00
25.00	720	4.0	$ 91,060	3,271	$ 163,088	0.253	1.00	0.00
29.00	600	5.0	$ 94,700	3,118	$ 163,379	0.253	1.00	0.00
29.00	600	5.1	$ 94,800	3,122	$ 163,561	0.253	1.00	0.00
40.00	240	5.0	$ 100,520	2,884	$ 164,041	0.254	1.00	0.00
40.00	240	5.1	$ 100,620	2,888	$ 164,223	0.255	1.00	0.00
30.00	600	4.0	$ 95,800	3,121	$ 164,538	0.255	1.00	0.00
29.00	660	2.0	$ 94,580	3,181	$ 164,641	0.255	1.00	0.00
25.00	720	5.0	$ 92,060	3,308	$ 164,910	0.255	1.00	0.00
25.00	720	5.1	$ 92,160	3,312	$ 165,092	0.256	1.00	0.00
40.00	360	2.0	$ 103,280	2,822	$ 165,434	0.256	1.00	0.00
35.00	480	4.0	$ 100,540	2,972	$ 165,988	0.257	1.00	0.00
25.00	780	2.0	$ 91,940	3,371	$ 166,172	0.257	1.00	0.00
30.00	600	5.0	$ 96,800	3,158	$ 166,360	0.258	1.00	0.00

Figure 4.12 HOMER software cost analysis

Figure 4.12, indicates that the optimization of cost in sequence from least to high cost was simulated. The net present cost and the cost of energy were $166,360 and 0.258$ respectively which is very necessary for the PV standalone design for Multi-service Access Getway (MSAG) due to its better reliability and efficiency.

Furthermore, the price is free from fuel and other additional costs. Hence the analysis is applied by minimizing the total net present cost of the PV system taking into account the operation, maintenance cost, investment cost, replacement cost, converter, and batteries.

4.3.2. Sensitivity Results

The following Figures 4.13, 4.14, and 4.15 shows the different cost sensitivity results under the HOMER simulation. Figure 4.13 explains the total net present cost verses different irradiations. When the irradiation is increased the total net present cost is decreasing linearly the figure also demonstrates about the total production kWh/yr. when the total net present cost is decreased, the total annual production is increasing.

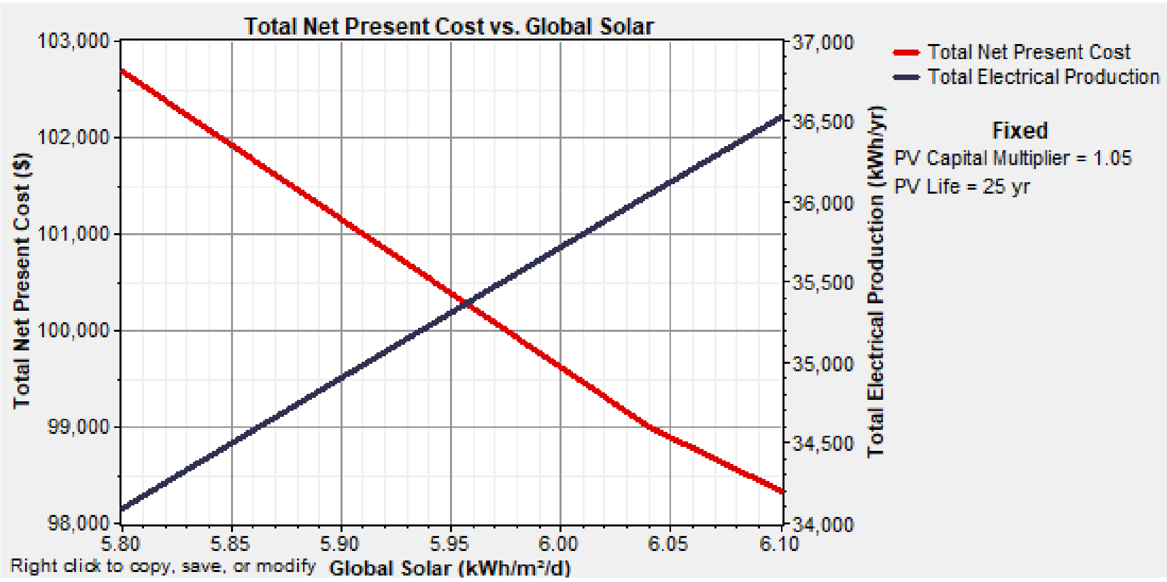

Figure 4.13 Total net present cost vs global solar

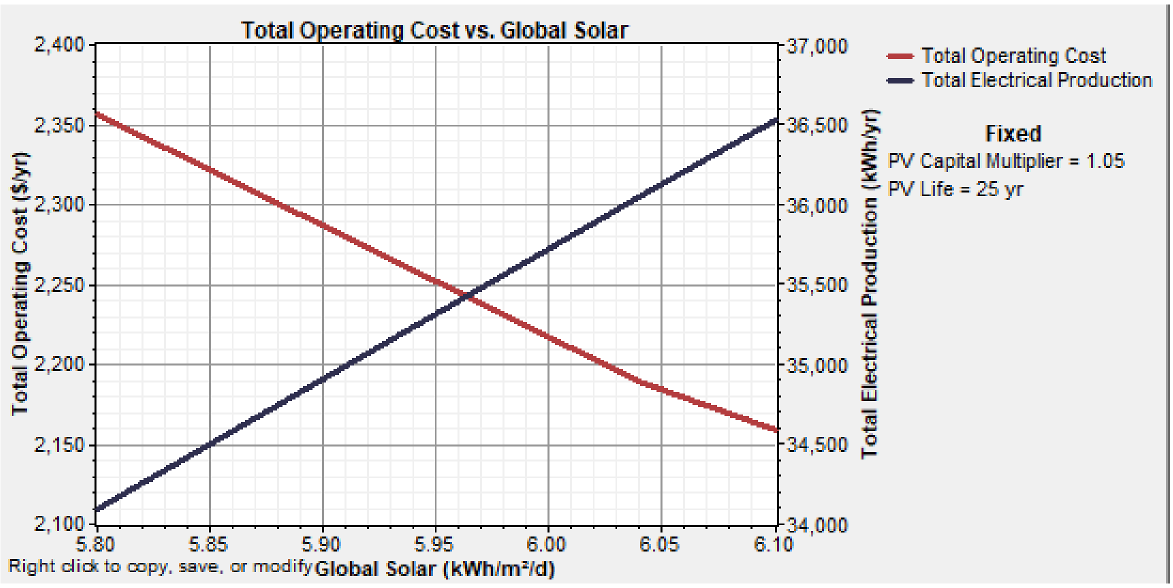

Figure 4.14 Total operating cost versus global solar

Figure 4.14 explains the total operating cost verses different irradiations. When the irradiation is increased the total operating cost is decreasing linearly as in the case of total net present cost. The figure also demonstrates about the total production kWh/yr. When the total operating cost is decreased as the irradiation increased, the total annual production is increasing.

The following Figure 4.15 explains about the carbon dioxide emission to the environment. When the total electrical energy production is increased the CO_2 is zero and this tells the designed PV system is fully renewable energy.

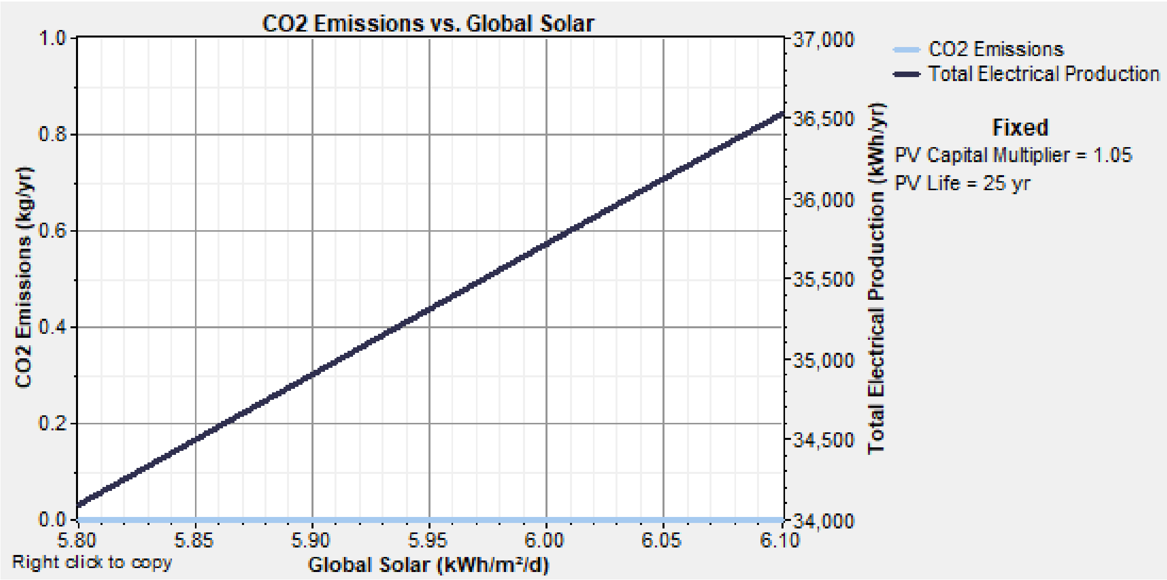

Figure 4.15 Carbon dioxide versus global solar

CHAPTER FIVE

CONCLUSION AND RECOMMENDATIONS

5.1. Conclusions

A stand-alone photovoltaic system which consists of PV arrays, battery, and power electronic converters for Ethio-telecom Multi-service Access Getway (MSAG) have been discussed. Also, the proposed system cost analysis both in mathematically and HOMER software which is an efficient for MSAG is done. Hence electricity from the Ethiopian electric utility (EEU) does not satisfy the demand of the community for wired telephone and internet applications.

Various significant components of the standalone PV system, such as sizing of the PV array, DC to DC converter modeling, maximum power tracking optimization (photovoltaic management) using P&O algorithm, and analysis of and battery management through the bidirectional converter and PI controllers were discussed. Finally for the implementation purpose the different components of overall system were modeled and implemented using MATLAB/Simulink. The appropriate sizes of standalone PV system elements were applied and the models are simulated based on the mathematical analysis. The battery bidirectional DC-DC converter and the charging/discharging of the battery are also studied. A bidirectional converter is used to manage the power flow between the DC bus and battery with a DC-link voltage.

Photovoltaic array, P&O for MPPT, and a bidirectional DC-DC converter have been described. A load voltage is regulated at 120V by a convectional PI controller. The standalone PV system management proves: when the power demand is more than the PV generation, the battery is discharging and provides the extra power and when photovoltaic generation is more than the power demand, the battery is charging.

Through the convectional PI controller, the standalone energy management system, the operation of battery charging and discharging were discussed. Also, the cost analysis was discussed using HOMER PRO software. The cost of energy was $0.258/kWh which is, reliable and efficient. It is to be noted that, this price is enough as compared to the current unit cost of electricity in Ethiopia. PV energy generation for the MSAG is very crucial and important due to its better efficiency and reliability to the power distribution for the MSAG. This price is also free from interruption and fuel cost.

Generally, the standalone photovoltaic system was simulated both in MATLAB and HOMER softwares by applying energy balance between the load demand and energy sources.

5.2. Recommendation

Energy is very important to accomplish different activities in human beings. Therefore, to improve energy crises especially in MSAG like devices which operates for 24hrs., the microgrid energy management standalone system has great contribution. Hence, in this thesis work the better energy control systems like fuzzy logic, GA, and PSO were not applied. In order to have a reliable control mechanisms and regulated output results the artificial intelligence optimization techniques are recommended.

As a final remark, the respective governments should get involved in providing financial support for procurement, installation of the PV system, encourage the use of microgrid energy management PV solar energy, make it a popular choice, and propagate this energy solution for a clinic, commercial, and buildings.

Reference

A. Tadessie, "Feasibility Study of Small Hydro/PV/Wind Hybrid System for Off-Grid Rural Electrification in Ethiopia," AAU, Addis Ababa Institute of Technology Master's Thesis, Power Engineering Stream, May 2011.

Andreas Nyman and Henrik Ekstrom, "Modeling of the Lithium-ion Battery," January,2012.

B. Fola, "Design and Analysis of Solar Powered Multilevel Inverter Fed Induction Motor Drive for Water Pumping Application (Case Study on Koka in Adama, South-East Ethiopia)", Adama Ethiopia, MSc.Thesis, October, 2020

Baron, D. (2010). The Impact of Telecommunications Services on Doing Business in Ethiopia. Addis Ababa Chamber of Commerce and Sectoral Associations.

Cisco Networking Academy, "Connecting Networks", First Edition, Cisco Press, May 2014.

Core Network, Retrieved on June 15, 2016, from https://en.wikipedia.org.

D. A. R. y. m. K Pooja, "Bidirectional DC-DC Converter for Solar Battery Backup Applications," IEEE, Vols. Vol. 06, , no. 02, pp. pp.-47-52, 2020.

D. K. Sharma, "Analysis of the Effect of Fill Factor on the Efficiency of Solar PV System for Improved Design of MPPT," in Department of Electronics & Comm. Engg, Udaipur INDIA, 2014.

D. W. Hart, Power electronics, Book.

Dalelo and A., "Rural Electrification in Ethiopia," Opportunities and Bottlenecks, Addis Ababa University, College of Education, 2003.

Deepak Ravi, Bandi Mallikarjuna Reddy, Shimi S.L., Paulson Samuel, "Bidirectional dc to dc converters: An Overview of Various Topologies, Switching Schemes and Control Techniques," International Journal of Engineering and Technology, vol. 7, no. 4.5, pp. 360-365, 2018.

Emma Raszmann, Kyri Baker, Ying Shi and Dane Christensen, " Modeling Stationary Lithium-Ion Batteries for Optimization and Predictive Control," IEEE Power and Energy Conference Champaign, February 23-24, 2017.

Ethiopia, Mean Annuaul Surplus of Water in Available from: https:// energy pedia. info/wiki/File: Mean Annual Water Surplus in Ethiopia.jpg.

Ethiopian Electrical Power in December 2016.

F. Liu, S. Duan and Y. Kang, "A Variable Step Size INC MPPT Method for PV System," IEEE Trans. Ind. Electron. Vols. 55, No. 7, pp. 2622-2628, July 2008.

Goggin, G. (2012). Cell phone culture: Mobile technology in everyday life. Routledge.

H. M. Mohammad Aman Yaqobi, "Control and Energy Management Strategy of Standalone DC Microgrid Cluster using PV and Battery Storage for Rural Application," IJPER, Vols. Vol. 2, No. 4, p. 53, 2018.

H. Mark, Stand-Alone Solar Electric Systems, 2010.

H. Raffel, "Realization of a Quasi-Direct Converter by a High Dynamic DC Link Voltage Regulator," PhD Thesis, University of Bremen, 2003.

http://www.ethiotelecom.et. (Accessed on July 08 ,2020).

I. Kashif and S. Zainal, "An Improved Modeling Method to Determine the Model Parameters of Photovoltaic Models Using Differential Evolution," Science-Direct, Solar Energy, Elsevier Ltd., vol. 85, pp. 2349-23359, 2011.

I. Sefa and I. Altin, "Grid Interactive Photovoltaic Inverters-a Review," JFac Eng Archit Gazi Univ, pp. 24(3):409-24, 2017.

I. Sefa, M. Demirtas and I. Colak, "Applications of One Axis Sun Tracking System," Energy Convers Manage, pp. 50:2709-18, 2015.

I. Z. M. N. Mohd Shawal Jadin, "A Sizing tool for PV Standalone System," Journal of Engineering and Applied Sciences, Vols. VOL. 10, NO. 22, pp. pp 1819-6608, 2015.

J. Abdul, A. Nazar. and A. R. Omega, "Simulation on Maximum Power Point Tracking of the Photovoltaic module Using LabView," International Journal of Advanced Research in Electrical, Electronics and Instrumentation Engineering, vol. 1(3), pp. 190-199, 2012.

J. Ejury, "Buck Converter Design," Infineon Technologies North America (ITNA), Durham, January 2013.

J. Grant, "Design and Simulation of a DC Microgrid for a Small Island in Belize," Sustainable Energy Engineering – Iceland School of Energy, 2018.

J. Lee, H. Bae and B. Cho, "Advanced Incremental Conductance MPPT Algorithm with A Variable Step Size," 12th International Power Electronics and Motion Control Conference EPE-PEMC, Vols. 65, No. 6, pp. 603-607, Aug. 2006.

J. Malla, R. Mohana, K. S. Manoj and K. S. Pravat, "Study of PV Based Water Pumping System for Agricultural Sector," Mater. Today, Proc., Vols. 5, No.1, pp. 1008-1016, 2018.

Kou-Bin Liu, Chen-Yao Liu and Yi-Hua Liu, " Analysis and controller design of a universal bidirectional dc-dc converter," energies, 2016.

L. H. L. N. S. D. I. Yen Yee Chia, " A load predictive energy management system for supercapacitor-battery hybrid energy storage system in solar application using the Support Vector Machine," Journal Applied Energy, no. 137, pp. 588-602, 2015.

L. Tolbert, F. Peng and T. Habetler, "Multivel converters for Large Electric Drives," IEEE Trans. Ind. Applicat., vol. 35, pp. 36-44, Jan/Feb. 2015.

Low Wen Yao, Aziz, J. A., Pui Yee Kong, N. R. N. Idris, " Modeling of Lithium-Ion Battery Using MATLAB/Simulink," in Low Wen Yao, Skudai, Johor, Malaysia, 09 February 2014 IEEE.

Lu L.,Han X.,Li J.,Hua J. and Ouyang M., "A review on the key issues for lithium-ion battery management in electric vehicles," Journal of Power Sources, no. 0378-7, p. 272–288, 2012.

M. B. Kumar, " Modeling and Control of PV/Wind," Halmstad University, 2017.

M. Boxwell, "Solar Electricity Handbook," Green stream Publishing, United Kingdom Ltd, 2017.

M. M. Gilbert, "Renewable and Efficient Electric Power System," Stanford University, Wiley and Sons, Inc., Hoboken, New Jersey, April 2004.

M. Martino, "Intelligent Control for Distributed System," 2012.

M. Parimita, M. Tariq and K. Mohan, Solar Photovoltaic System Applications, 2016.

M. Rivera, "Small Wind / Photovoltaic Hybrid Renewable Energy System Optimization," MSc Thesis, University of Puerto Rico., Puerto Rico, 2008.

M. S. Rahman, "Buck Converter Design Issues," Master Thesis, Linkoping Institute of Technology, 2007.

M.-C. T. C.-H. H. Y.-G. L. Kuei-Hsiang Chao, "Design and Implementation of a Bidirectional DC-DC Converter for Stand-alone Photovoltaic Systems," International Journal of Computer, Consumer and Control (IJ3C), vol. 2, no. 3, 2013.

N. Argaw, R. Forester and A. Ellis, "Renewable Energy for Water Pumping Applications in Rural, National Renewable Energy Laboratory, Villages," pp. 19-26, July 2003.

N. Mohan and T. M. Undeland, Power Electronics, Converters, Applications and Design: Wiley-India,2007.

Panels, the Photovoltaic Panels Work Available from: http:/www.Irc.rpi.edu/ programs/nlpip/lightingAnswers/photovoltaic/04-photovoltaic-panels-work.asp.

Panels, the Planet's most Powerful Available from: http://us.sunpowercorp.com/ homes/sunpoweradvantage/more-electricity.

Priscilla Oppenheimer, “Top-Down Network Design”, Third Edition, Cisco Press, 2012.

R. S. Burns, Advanced Control Engineering, 2001.

R.A. Dougal, S. Liu, R.E. White, "“Power and Life Extension of Battery Ultra-capacitor Hybrids”," IEEE Transactions on Component and Packaging Technologies, vol. 25, no. 1, p. 120-131, 2002.

S. A. S. A. A. L. -J. UBOORI, "Stand-Alone Photovoltaic System," Energy Sci. & Tech., vol. vol.6, 2016.

S. W. P. H. C. M. G. R. M. T. K. B. B. G. J. Kitson, "Modeling of an expandable, reconfigurable, renewable DC microgrid for off-grid communities," in Energy, 2019.

Salih, T., Wang, Y., and Ahmed Adam, M.A. (2014). Renewable Micro Hybrid System of Solar Panel and Wind Turbine for Telecommunication Equipment in Remote Areas in Sudan. Energy Procedia 61, 80 – 83.

Shafinaz A. Lopa, S. Hossain, M. K. Hasan, and T. K. Chakraborty, "Design and Simulation of DC - DC Converters," International Research Journal of Engineering and Technology (IRJET), vol. 03, no. 01, pp. 2395 - 0072, Jan-2016.

T. Huan-Liang and S. Yi-Jie, "Development of Generalized Photovoltaic Model Using Matlab/Simulink," Proceedings of the World Congress on Engineering and Computer Science, San Fransico, USA, October 22-24 2008.

T. K. S. Z. H. Radu-Emil Precup, Solar Photovoltaic Power Plants, Springer, 2019.

T. M. Parimita Mohanty, Solar Photovoltaic System Applications, Springer International Publishing Switzerland, 2016.

The Radicati Group, INC. (2014-2018). Mobile Statistics, Technology Market Research Firm. PALO ALTO, CA, USA

U. Report, "Eastern and Southern Africa Available from: https://www.unicef.org".

UmaShankar Patel, Ms. Dhaneshwari Sahu, Deepkiran Tirkey, "Maximum Power Point Tracking Using & Observe Algorithm and Compare With another Algorithm," International Journal of Digital Application & Contemporary research, vol. 2, no. 2, 2013.

V. Quaschning, Renewable Energy and Climate Change, John Wiley and Sons, 2010.

Y. D. X. H. P. K. R. C. B. Abhishek Kumar, "Energy management system controller for a rural microgrid," The Journal of Engineering, 2017.

Appendix

Appendix A: MSAG

Appendix B: HOMER Software results

PV (kW)	H200	Conv. (kW)	Initial Capital	Operating Cost ($/yr)	Total NPC	COE ($/kWh)	Ren. Frac.	Capacity Shortage
15.00	360	2.0	$ 50,780	2,159	$ 98,324	0.155	1.00	0.06
15.00	240	2.0	$ 45,020	2,451	$ 99,007	0.160	1.00	0.14
18.00	240	2.0	$ 51,320	2,274	$ 101,402	0.161	1.00	0.08
15.00	360	4.0	$ 52,780	2,233	$ 101,967	0.161	1.00	0.06
13.00	240	2.0	$ 40,820	2,787	$ 102,203	0.171	1.00	0.23
13.00	360	2.0	$ 46,580	2,530	$ 102,304	0.167	1.00	0.16
15.00	240	4.0	$ 47,020	2,526	$ 102,650	0.166	1.00	0.14
18.00	360	2.0	$ 57,080	2,113	$ 103,608	0.162	1.00	0.02
15.00	360	5.0	$ 53,780	2,271	$ 103,789	0.164	1.00	0.06
15.00	360	5.1	$ 53,880	2,274	$ 103,971	0.164	1.00	0.06
15.00	240	5.0	$ 48,020	2,563	$ 104,472	0.169	1.00	0.14
15.00	240	5.1	$ 48,120	2,567	$ 104,654	0.170	1.00	0.14
20.00	240	2.0	$ 55,520	2,242	$ 104,895	0.165	1.00	0.05
18.00	240	4.0	$ 53,320	2,349	$ 105,045	0.167	1.00	0.08
15.00	480	2.0	$ 56,540	2,216	$ 105,343	0.165	1.00	0.02
13.00	240	4.0	$ 42,820	2,862	$ 105,846	0.177	1.00	0.23
13.00	360	4.0	$ 48,580	2,605	$ 105,947	0.173	1.00	0.16
18.00	240	5.0	$ 54,320	2,386	$ 106,867	0.170	1.00	0.08
18.00	240	5.1	$ 54,420	2,390	$ 107,049	0.170	1.00	0.08
18.00	360	4.0	$ 59,080	2,187	$ 107,251	0.167	1.00	0.02
13.00	240	5.0	$ 43,820	2,899	$ 107,668	0.180	1.00	0.23
13.00	360	5.0	$ 49,580	2,642	$ 107,769	0.176	1.00	0.16
13.00	240	5.1	$ 43,920	2,903	$ 107,850	0.181	1.00	0.23
13.00	360	5.1	$ 49,680	2,646	$ 107,951	0.176	1.00	0.16
20.00	360	2.0	$ 61,280	2,143	$ 108,478	0.169	1.00	0.01
20.00	240	4.0	$ 57,520	2,317	$ 108,538	0.171	1.00	0.05
15.00	480	4.0	$ 58,540	2,291	$ 108,986	0.170	1.00	0.02

PV (kW)	H200	Conv. (kW)	Initial Capital	Operating Cost ($/yr)	Total NPC	COE ($/kWh)	Ren. Frac.	Capacity Shortage
15.00	600	5.0	$ 65,300	2,618	$ 122,946	0.191	1.00	0.01
15.00	600	5.1	$ 65,400	2,621	$ 123,128	0.192	1.00	0.01
20.00	480	5.0	$ 70,040	2,442	$ 123,825	0.192	1.00	0.01
15.00	660	2.0	$ 65,180	2,664	$ 123,858	0.192	1.00	0.01
20.00	480	5.1	$ 70,140	2,446	$ 124,007	0.193	1.00	0.01
13.00	600	4.0	$ 60,100	2,959	$ 125,267	0.201	1.00	0.10
18.00	600	2.0	$ 68,600	2,589	$ 125,611	0.195	1.00	0.00
25.00	360	4.0	$ 73,780	2,363	$ 125,826	0.195	1.00	0.01
13.00	600	5.0	$ 61,100	2,996	$ 127,089	0.204	1.00	0.10
13.00	600	5.1	$ 61,200	3,000	$ 127,271	0.204	1.00	0.10
15.00	660	4.0	$ 67,180	2,739	$ 127,501	0.198	1.00	0.01
29.00	240	2.0	$ 74,420	2,411	$ 127,526	0.199	1.00	0.02
13.00	660	2.0	$ 60,980	3,025	$ 127,600	0.204	1.00	0.10
25.00	360	5.0	$ 74,780	2,401	$ 127,647	0.198	1.00	0.01
25.00	360	5.1	$ 74,880	2,404	$ 127,830	0.199	1.00	0.01
18.00	600	4.0	$ 70,600	2,663	$ 129,255	0.201	1.00	0.00
15.00	660	5.0	$ 68,180	2,776	$ 129,323	0.201	1.00	0.01
15.00	660	5.1	$ 68,280	2,780	$ 129,505	0.201	1.00	0.01
30.00	240	2.0	$ 76,520	2,442	$ 130,292	0.203	1.00	0.02
15.00	720	2.0	$ 68,060	2,830	$ 130,385	0.202	1.00	0.01
18.00	600	5.0	$ 71,600	2,701	$ 131,076	0.203	1.00	0.00
29.00	240	4.0	$ 76,420	2,486	$ 131,169	0.204	1.00	0.02
13.00	660	4.0	$ 62,980	3,100	$ 131,243	0.210	1.00	0.10
18.00	600	5.1	$ 71,700	2,704	$ 131,259	0.204	1.00	0.00
20.00	600	2.0	$ 72,800	2,662	$ 131,416	0.204	1.00	0.00
18.00	660	2.0	$ 71,480	2,754	$ 132,138	0.205	1.00	0.00
25.00	480	2.0	$ 77,540	2,514	$ 132,906	0.206	1.00	0.00

PV (kW)	H200	Conv. (kW)	Initial Capital	Operating Cost ($/yr)	Total NPC	COE ($/kWh)	Ren. Frac.	Capacity Shortage
18.00	360	5.0	$ 60,080	2,225	$ 109,073	0.170	1.00	0.02
18.00	360	5.1	$ 60,180	2,228	$ 109,255	0.170	1.00	0.02
13.00	480	2.0	$ 52,340	2,614	$ 109,910	0.177	1.00	0.12
20.00	240	5.0	$ 58,520	2,354	$ 110,360	0.174	1.00	0.05
20.00	240	5.1	$ 58,620	2,358	$ 110,542	0.174	1.00	0.05
15.00	480	5.0	$ 59,540	2,328	$ 110,808	0.173	1.00	0.02
15.00	480	5.1	$ 59,640	2,332	$ 110,990	0.173	1.00	0.02
20.00	360	4.0	$ 63,280	2,218	$ 112,121	0.175	1.00	0.01
18.00	480	2.0	$ 62,840	2,257	$ 112,545	0.175	1.00	0.01
13.00	480	4.0	$ 54,340	2,689	$ 113,553	0.183	1.00	0.12
20.00	360	5.0	$ 64,280	2,255	$ 113,943	0.177	1.00	0.01
20.00	360	5.1	$ 64,380	2,259	$ 114,125	0.178	1.00	0.01
13.00	480	5.0	$ 55,340	2,726	$ 115,374	0.186	1.00	0.12
13.00	480	5.1	$ 55,440	2,730	$ 115,557	0.186	1.00	0.12
18.00	480	4.0	$ 64,840	2,332	$ 116,189	0.181	1.00	0.01
25.00	240	2.0	$ 66,020	2,306	$ 116,816	0.183	1.00	0.03
15.00	600	2.0	$ 62,300	2,506	$ 117,481	0.183	1.00	0.01
18.00	480	5.0	$ 65,840	2,369	$ 118,010	0.183	1.00	0.01
18.00	480	5.1	$ 65,940	2,373	$ 118,192	0.184	1.00	0.01
20.00	480	2.0	$ 67,040	2,330	$ 118,360	0.184	1.00	0.01
25.00	240	4.0	$ 68,020	2,381	$ 120,459	0.188	1.00	0.03
15.00	600	4.0	$ 64,300	2,580	$ 121,124	0.188	1.00	0.01
13.00	600	2.0	$ 58,100	2,884	$ 121,624	0.195	1.00	0.10
20.00	480	4.0	$ 69,040	2,405	$ 122,004	0.189	1.00	0.01
25.00	360	2.0	$ 71,780	2,289	$ 122,182	0.190	1.00	0.01
25.00	240	5.0	$ 69,020	2,418	$ 122,281	0.191	1.00	0.03
25.00	240	5.1	$ 69,120	2,422	$ 122,463	0.191	1.00	0.03

PV (kW)	H200	Conv. (kW)	Initial Capital	Operating Cost ($/yr)	Total NPC	COE ($/kWh)	Ren. Frac.	Capacity Shortage
29.00	240	5.0	$ 77,420	2,523	$ 132,991	0.207	1.00	0.02
13.00	660	5.0	$ 63,980	3,137	$ 133,065	0.213	1.00	0.10
29.00	240	5.1	$ 77,520	2,527	$ 133,173	0.207	1.00	0.02
13.00	660	5.1	$ 64,080	3,141	$ 133,247	0.213	1.00	0.10
29.00	360	2.0	$ 80,180	2,427	$ 133,630	0.207	1.00	0.01
13.00	720	2.0	$ 63,860	3,175	$ 133,778	0.214	1.00	0.09
30.00	240	4.0	$ 78,520	2,516	$ 133,935	0.208	1.00	0.02
15.00	720	4.0	$ 70,060	2,905	$ 134,028	0.208	1.00	0.01
20.00	600	4.0	$ 74,800	2,736	$ 135,060	0.209	1.00	0.00
30.00	240	5.0	$ 79,520	2,554	$ 135,757	0.211	1.00	0.02
18.00	660	4.0	$ 73,480	2,829	$ 135,782	0.211	1.00	0.00
15.00	720	5.0	$ 71,060	2,942	$ 135,850	0.211	1.00	0.01
30.00	240	5.1	$ 79,620	2,557	$ 135,939	0.212	1.00	0.02
15.00	720	5.1	$ 71,160	2,946	$ 136,032	0.211	1.00	0.01
30.00	360	2.0	$ 82,280	2,463	$ 136,516	0.212	1.00	0.00
25.00	480	4.0	$ 79,540	2,589	$ 136,549	0.212	1.00	0.00
20.00	600	5.0	$ 75,800	2,774	$ 136,881	0.212	1.00	0.00
15.00	780	2.0	$ 70,940	2,998	$ 136,960	0.213	1.00	0.01
20.00	600	5.1	$ 75,900	2,777	$ 137,064	0.213	1.00	0.00
29.00	360	4.0	$ 82,180	2,502	$ 137,274	0.213	1.00	0.01
13.00	720	4.0	$ 65,860	3,249	$ 137,421	0.220	1.00	0.09
18.00	660	5.0	$ 74,480	2,866	$ 137,603	0.213	1.00	0.00
18.00	660	5.1	$ 74,580	2,870	$ 137,786	0.214	1.00	0.00
20.00	660	2.0	$ 75,680	2,827	$ 137,939	0.214	1.00	0.00
15.00	792	2.0	$ 71,516	3,031	$ 138,270	0.215	1.00	0.01
25.00	480	5.0	$ 80,540	2,626	$ 138,371	0.215	1.00	0.00
25.00	480	5.1	$ 80,640	2,630	$ 138,553	0.215	1.00	0.00

PV (kW)	H200	Conv. (kW)	Initial Capital	Operating Cost ($/yr)	Total NPC	COE ($/kWh)	Ren. Frac.	Capacity Shortage
18.00	720	2.0	$ 74,360	2,920	$ 138,663	0.215	1.00	0.00
29.00	360	5.0	$ 83,180	2,539	$ 139,095	0.216	1.00	0.01
13.00	720	5.0	$ 66,860	3,287	$ 139,243	0.222	1.00	0.09
29.00	360	5.1	$ 83,280	2,543	$ 139,277	0.216	1.00	0.01
13.00	720	5.1	$ 66,960	3,290	$ 139,425	0.223	1.00	0.09
13.00	780	2.0	$ 66,740	3,329	$ 140,058	0.223	1.00	0.09
30.00	360	4.0	$ 84,280	2,537	$ 140,160	0.217	1.00	0.00
15.00	780	4.0	$ 72,940	3,072	$ 140,603	0.218	1.00	0.01
13.00	792	2.0	$ 67,316	3,361	$ 141,337	0.225	1.00	0.09
20.00	660	4.0	$ 77,680	2,902	$ 141,582	0.219	1.00	0.00
15.00	792	4.0	$ 73,516	3,106	$ 141,913	0.220	1.00	0.01
30.00	360	5.0	$ 85,280	2,575	$ 141,981	0.220	1.00	0.00
30.00	360	5.1	$ 85,380	2,578	$ 142,164	0.221	1.00	0.00
18.00	720	4.0	$ 76,360	2,994	$ 142,306	0.221	1.00	0.00
15.00	780	5.0	$ 73,940	3,110	$ 142,425	0.221	1.00	0.01
15.00	780	5.1	$ 74,040	3,113	$ 142,607	0.221	1.00	0.01
20.00	660	5.0	$ 78,680	2,939	$ 143,404	0.222	1.00	0.00
20.00	660	5.1	$ 78,780	2,943	$ 143,586	0.223	1.00	0.00
13.00	780	4.0	$ 68,740	3,404	$ 143,701	0.229	1.00	0.09
15.00	792	5.0	$ 74,516	3,143	$ 143,735	0.223	1.00	0.01
15.00	792	5.1	$ 74,616	3,147	$ 143,917	0.223	1.00	0.01
18.00	720	5.0	$ 77,360	3,032	$ 144,128	0.223	1.00	0.00
35.00	240	2.0	$ 87,020	2,599	$ 144,263	0.224	1.00	0.01
18.00	720	5.1	$ 77,460	3,035	$ 144,310	0.224	1.00	0.00
20.00	720	2.0	$ 78,560	2,996	$ 144,540	0.224	1.00	0.00
29.00	480	2.0	$ 85,940	2,664	$ 144,619	0.224	1.00	0.00
13.00	792	4.0	$ 69,316	3,436	$ 144,980	0.231	1.00	0.09

PV (kW)	H200	Conv. (kW)	Initial Capital	Operating Cost ($/yr)	Total NPC	COE ($/kWh)	Ren. Frac.	Capacity Shortage
18.00	780	2.0	$ 77,240	3,091	$ 145,306	0.225	1.00	0.00
13.00	780	5.0	$ 69,740	3,441	$ 145,523	0.232	1.00	0.09
13.00	780	5.1	$ 69,840	3,445	$ 145,705	0.232	1.00	0.09
25.00	600	2.0	$ 83,300	2,847	$ 145,995	0.226	1.00	0.00
18.00	792	2.0	$ 77,816	3,126	$ 146,651	0.227	1.00	0.00
13.00	792	5.0	$ 70,316	3,473	$ 146,802	0.234	1.00	0.09
13.00	792	5.1	$ 70,416	3,477	$ 146,984	0.234	1.00	0.09
30.00	480	2.0	$ 88,040	2,702	$ 147,548	0.229	1.00	0.00
35.00	240	4.0	$ 89,020	2,674	$ 147,907	0.230	1.00	0.01
20.00	720	4.0	$ 80,560	3,071	$ 148,184	0.230	1.00	0.00
29.00	480	4.0	$ 87,940	2,739	$ 148,263	0.230	1.00	0.00
18.00	780	4.0	$ 79,240	3,165	$ 148,949	0.231	1.00	0.00
25.00	600	4.0	$ 85,300	2,921	$ 149,638	0.232	1.00	0.00
35.00	240	5.0	$ 90,020	2,711	$ 149,728	0.233	1.00	0.01
35.00	240	5.1	$ 90,120	2,715	$ 149,910	0.233	1.00	0.01
20.00	720	5.0	$ 81,560	3,108	$ 150,005	0.232	1.00	0.00
29.00	480	5.0	$ 88,940	2,776	$ 150,084	0.233	1.00	0.00
20.00	720	5.1	$ 81,660	3,112	$ 150,187	0.233	1.00	0.00
29.00	480	5.1	$ 89,040	2,780	$ 150,266	0.233	1.00	0.00
18.00	792	4.0	$ 79,816	3,200	$ 150,295	0.233	1.00	0.00
18.00	780	5.0	$ 80,240	3,203	$ 150,771	0.234	1.00	0.00
35.00	360	2.0	$ 92,780	2,640	$ 150,920	0.234	1.00	0.00
18.00	780	5.1	$ 80,340	3,206	$ 150,953	0.234	1.00	0.00
30.00	480	4.0	$ 90,040	2,777	$ 151,192	0.234	1.00	0.00
20.00	780	2.0	$ 81,440	3,171	$ 151,268	0.234	1.00	0.00
25.00	600	5.0	$ 86,300	2,959	$ 151,460	0.235	1.00	0.00
25.00	600	5.1	$ 86,400	2,962	$ 151,642	0.235	1.00	0.00

PV (kW)	H200	Conv. (kW)	Initial Capital	Operating Cost ($/yr)	Total NPC	COE ($/kWh)	Ren. Frac.	Capacity Shortage
18.00	792	5.0	$ 80,816	3,238	$ 152,116	0.236	1.00	0.00
18.00	792	5.1	$ 80,916	3,241	$ 152,298	0.236	1.00	0.00
20.00	792	2.0	$ 82,016	3,206	$ 152,613	0.236	1.00	0.00
25.00	660	2.0	$ 86,180	3,021	$ 152,718	0.237	1.00	0.00
30.00	480	5.0	$ 91,040	2,814	$ 153,013	0.237	1.00	0.00
30.00	480	5.1	$ 91,140	2,818	$ 153,196	0.237	1.00	0.00
35.00	360	4.0	$ 94,780	2,715	$ 154,564	0.240	1.00	0.00
20.00	780	4.0	$ 83,440	3,245	$ 154,911	0.240	1.00	0.00
20.00	792	4.0	$ 84,016	3,280	$ 156,256	0.242	1.00	0.00
25.00	660	4.0	$ 88,180	3,096	$ 156,361	0.242	1.00	0.00
35.00	360	5.0	$ 95,780	2,752	$ 156,385	0.242	1.00	0.00
35.00	360	5.1	$ 95,880	2,756	$ 156,567	0.243	1.00	0.00
20.00	780	5.0	$ 84,440	3,283	$ 156,733	0.243	1.00	0.00
20.00	780	5.1	$ 84,540	3,286	$ 156,915	0.243	1.00	0.00
29.00	600	2.0	$ 91,700	3,007	$ 157,914	0.245	1.00	0.00
20.00	792	5.0	$ 85,016	3,318	$ 158,078	0.245	1.00	0.00
25.00	660	5.0	$ 89,180	3,133	$ 158,183	0.245	1.00	0.00
20.00	792	5.1	$ 85,116	3,321	$ 158,260	0.245	1.00	0.00
25.00	660	5.1	$ 89,280	3,137	$ 158,365	0.245	1.00	0.00
40.00	240	2.0	$ 97,520	2,772	$ 158,576	0.246	1.00	0.00
25.00	720	2.0	$ 89,060	3,196	$ 159,445	0.247	1.00	0.00
30.00	600	2.0	$ 93,800	3,047	$ 160,895	0.249	1.00	0.00
29.00	600	4.0	$ 93,700	3,081	$ 161,557	0.250	1.00	0.00
40.00	240	4.0	$ 99,520	2,847	$ 162,220	0.252	1.00	0.00
35.00	480	2.0	$ 98,540	2,897	$ 162,345	0.252	1.00	0.00
25.00	720	4.0	$ 91,060	3,271	$ 163,088	0.253	1.00	0.00
29.00	600	5.0	$ 94,700	3,118	$ 163,379	0.253	1.00	0.00

Appendix C: MATLAB Simulink data

MATLAB codes for maximum power point tracking algorithm (P&O).

```
function duty = MPPT_control (V, I, deltaD_in)
duty_init = 0.05;
duty_min = 0;
duty_max = 0.75;
persistent Vold Pold duty_old;
if isempty (Vold)
   Vold = 0;
   Pold = 0;
   duty_old = duty_init;
end
P = V*I;
dV = V- Vold;
dP = P- Pold;
duty = duty_old;
deltaD = deltaD_in;
if dP ~= 0
   if dP < 0
      if dV < 0
         duty = duty_old - deltaD;
      else
         duty = duty_old + deltaD;
      end
   else
      if dV < 0
         duty = duty_old + deltaD;
      else
         duty = duty_old - deltaD;
      end
   end
end
```

```
if duty >= duty_max
   duty = duty_max;
elseif duty < duty_min
   duty = duty_min;
end
duty_old = duty;
Vold = V;
Pold = P;
```

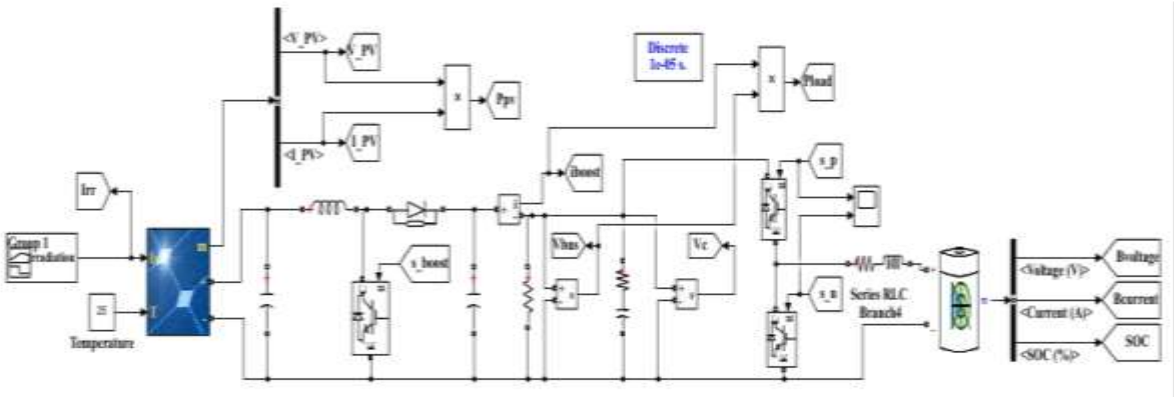

Figure C1. The proposed system simulation in MATLAB

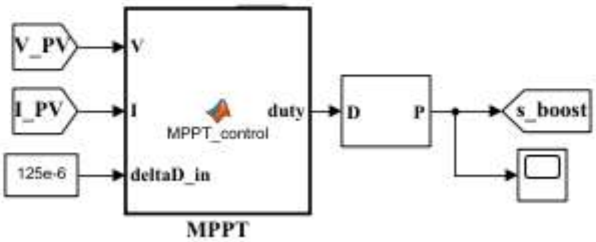

Figure C2. The MPPT P&O Algorithm in MATLAB/Simulink

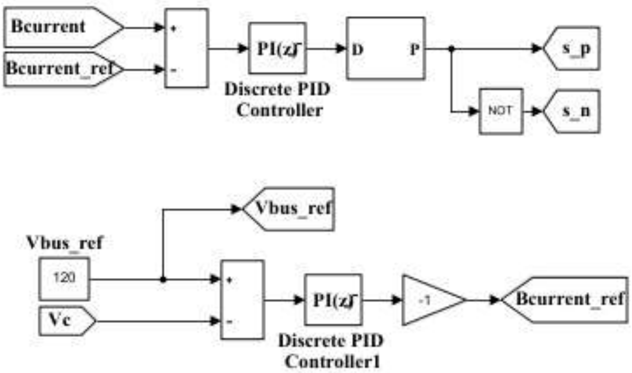

Figure C3. The battery charging and discharging control

Appendix D: Battery storage specifications

DC12-200 (12V200Ah)

DC (Deep Cycle) series is specially designed for frequent cyclic discharge. By using strong grids and specially designed active material, the DC series battery offers 30% more cyclic life than the standby series. It is suitable for solar energy systems, marine and RV etc.

Specification

Cells Per Unit	6
Voltage Per Unit	12
Capacity	200Ah@10hr-rate to 1.80V per cell @25℃
Weight	Approx. 60.0 Kg (Tolerance±1.5%)
Max. Discharge Current	2000 A (5 sec)
Internal Resistance	Approx. 4 mΩ
Operating Temperature Range	Discharge: -20℃~60℃ Charge: 0℃~50℃ Storage: -20℃~60℃
Normal Operating Temperature Range	25℃±5℃
Float charging Voltage	13.6 to 13.8 VDC/unit Average at 25℃
Recommended Maximum Charging Current	60 A
Equalization and Cycle Service	14.6 to 14.8 VDC/unit Average at 25℃
Self Discharge	RITAR Valve Regulated Lead Acid (VRLA) batteries can be stored for more than 6 months at 25℃. Self-discharge ratio less than 3% per month at 25℃. Please charge batteries before using.
Terminal	Terminal F10
Container Material	A.B.S. UL94-HB, UL94-V0 Optional.